

# State-dependence of climate sensitivity: attractor constraints and palaeoclimate regimes

Anna S. von der Heydt<sup>\*†</sup>      Peter Ashwin<sup>‡</sup>

October 23, 2021

## Abstract

Equilibrium climate sensitivity is a measure that is frequently used to predict long-term climate change. It is, however, not very well constrained, with both climate models and observational data suggesting a rather large uncertainty on climate sensitivity. The reasons for this include: the climate has a strong internal variability on many time scales, it is subject to a non-stationary forcing and it is, on many timescales, out of equilibrium with the changes in the radiative forcing. Palaeo records and models of past climate variations give some insight into how the climate system responds to various forcings although care must be taken of the *slow* feedback processes before comparing palaeo climate sensitivity estimates with estimates from (short time scale) model simulations. In addition, for the late Pleistocene ice age cycles it has been shown from both proxy data and a conceptual climate model that climate sensitivity varies considerably between the cold and warm phases because the *fast* feedback processes can change their relative strength and time scales over one cycle. Consequently, another reason for large uncertainty on palaeo climate sensitivity may be the fact that it is strongly state- (and therefore time-) dependent.

Using a conceptual model of Gildor and Tziperman (2001) with Milankovich forcing and dynamical ocean biogeochemistry, we explore how climate sensitivity can be estimated from unperturbed and perturbed model time series. Even in this rather simple model we find a wide range of estimates of the distribution of climate sensitivity, depending on climate state and variability within the unperturbed attractor. For climate states perturbed by instantaneous doubling of  $\text{CO}_2$ , the sensitivity estimates agree with those for the unperturbed model after transient decay back to a “climate attractor”. In this sense, climate sensitivity can be seen as a distribution that is a local property of the climate attractor. We also follow the classical climate model approach to sensitivity, where  $\text{CO}_2$  is prescribed and non-dynamic. While we find again a strong

---

<sup>\*</sup>Institute for Marine and Atmospheric Research, Utrecht and Center for Extreme Matter and Emergent Phenomena, Utrecht University, Utrecht, the Netherlands.

<sup>†</sup>Correspondence: (A.S.vonderHeydt@uu.nl)

<sup>‡</sup>Centre for Systems, Dynamics and Control, Department of Mathematics, University of Exeter, Exeter EX4 4QF, UK.

dependence on the background climate using this approach, the climate sensitivity values are consistently smaller than those derived from the perturbed experiments with dynamic CO<sub>2</sub>. This suggests that climate sensitivity estimates from climate models may depend significantly on future dynamics, and not just the level of CO<sub>2</sub>.

# 1 Introduction

In order to estimate the potential anthropogenic impact on climate in the future the response of the climate system to perturbations needs to be quantified. A frequently used measure for the response to changes in atmospheric CO<sub>2</sub>-concentration is the equilibrium climate sensitivity (ECS), which is defined as the increase in global mean surface temperature per radiative forcing change after the fast-acting feedback processes in the Earth System had time to equilibrate [Charney, 1979]. It is mostly determined from climate model simulations where the atmospheric CO<sub>2</sub>-concentration is doubled within a few decades and equilibrium is assumed after typically 100-200 years. Any slow climate processes are kept stationary in these model simulations. ECS is a benchmark quantity in climate models but is still characterised by a considerable uncertainty of 1.5 – 4.5°C per CO<sub>2</sub>-doubling [IPCC, 2013]. Climate observations from the instrumental period have not narrowed down the range of expected climate change [Knutti and Hegerl, 2008]. In particular, large temperature changes as a consequence of atmospheric CO<sub>2</sub> increase cannot be excluded.

The observed warming of the Earth is not only the consequence of the direct radiative forcing due to changes in the atmospheric CO<sub>2</sub>-concentration, but is the result of a combination of often fast-acting (positive and negative) feedback mechanisms, mostly related to atmospheric water vapour content, sea-ice and cloud albedo and aerosol concentrations. On the slower (decadal) time scales ocean heat uptake also contributes to the forcing. Quantifying the complete forcing is therefore not an easy task and limits our ability to determine the exact value of climate sensitivity [Schwartz, 2012].

Another reason for the large uncertainty in the climate sensitivity is the fact that the climate has a strong internal variability on many time scales, is subject to a non-stationary forcing and mostly out of equilibrium with the changes in the radiative forcing. Even though climate models are improving in their ability to reproduce the present-day spatial and temporal structure of the climate, these models are mostly not validated against climate variability in past background climate states that are substantially different from the present-day climate. Moreover, the most appropriate concept for sensitivity in the presence of natural variability and forcing is still under debate, with recent work by Ghil and co-workers proposing a non-autonomous stochastic approach in terms of random dynamical systems [Ghil, 2013, Chekroun et al., 2011], and suggesting that climate sensitivity corresponds to a derivative of a metric (Wasserstein distance) evaluated for the invariant measure with respect to some parameter that is changed.

The distribution of possible values of ECS is not easy to reach with typical Earth system models due to the wide range of time scales covered by the different feedback processes. Therefore, in the most recent IPCC report [IPCC, 2013] an alternative method to determine

climate sensitivity is applied that does not require the model to be run to full equilibrium and uses a regression of the temperature change versus net radiative imbalance at the top of the atmosphere [Gregory et al., 2004]. This alternative method, however, still assumes the feedbacks in the climate system are constant, while on the longer time it is very likely that the feedbacks do depend on time (or background climate state), as has been suggested in many previous model studies, e.g., Senior and Mitchell [2000], Gregory et al. [2004], Crucifix [2006], Andrews and Forster [2008], Yoshimori et al. [2011], Caballero and Huber [2013], von der Heydt et al. [2014].

Another approach to detect whether the climate sensitivity (CS) depends on the background climate is to reconstruct CS from proxy data during periods when the background climate was different from today. The reconstructed temperature change involves, however, also other feedback processes on much slower time scales that are usually not considered in climate model studies, such as variations in land ice albedo or vegetation distributions. To this end, the term Earth System Sensitivity (ESS) has been introduced, which quantifies the long-term response in global mean surface temperature after an increase in atmospheric CO<sub>2</sub> including all Earth system feedbacks (except the carbon cycle feedbacks) and is generally larger than the ECS [Lunt et al., 2010, Haywood et al., 2013]. A recently developed framework how to determine climate sensitivity from palaeo data suggests that the ECS can, in principle, be estimated from the ESS, if all contributing slow feedback processes can be quantified [Rohling et al., 2012]. This means, however, that a lot more information than only atmospheric CO<sub>2</sub> and global mean temperature is necessary from the palaeo-record. To explicitly specify the slow processes included in the estimate palaeo climate sensitivity, the specific climate sensitivity  $S_{[A,B,...]}$  has been defined, where  $A, B, ...$  indicates the slow processes that have been taken into account, with the most practical version to be reconstructed from palaeodata being  $S_{[CO_2, LI]}$  ('LI' stands for the land-ice albedo forcing).

This paper explores the distribution of climate sensitivities from long time series, in order to compare palaeo-climate data and model-derived values. We use a conceptual model of the Earth system [Gildor and Tziperman, 2001, Gildor et al., 2002], that includes dynamic CO<sub>2</sub> and is able to simulate glacial-interglacial cycles as relaxation oscillations. In the presence of Milankovitch forcing, the model gives reasonably realistic timings and profiles of ice ages. The model contains a dynamic slow (land ice-albedo) and a fast (sea ice-albedo) feedback process. During glacial periods a lot of sea ice is present, which is the reason for a relatively large equilibrium climate sensitivity compared to the one during warm interglacial times when there is little or no sea ice to melt under increasing CO<sub>2</sub>. Along a full glacial-interglacial cycle, the model therefore shows a strong state dependency of the fast feedback processes in the equilibrium climate sensitivity, see von der Heydt et al. [2014].

The paper is organised as follows. In the remainder of this section we discuss fast and slow processes in the climate system and ways in which climate sensitivity can be interpreted as a property of an invariant measure on a "climate attractor". In Section 2 we introduce the specific conceptual climate model of the glacial-interglacial cycles. This model is perturbed in several ways along the glacial-interglacial cycles and the distribution of (state-dependent) climate sensitivity is discussed. In Section 3 we review different methods to extract the same

ECS from a long (glacial-interglacial) times series with the same model. We conclude in Section 3.3 with a discussion of some issues related to the extraction and interpretation of ECS from palaeo climate time series.

## 1.1 Fast and slow processes in the climate system

The global mean surface temperature of the Earth  $T$  is determined by the contributions of various processes (being external or internal to the climate system) to the radiative balance, so

$$\frac{dT}{dt} \sim R_{forcing} + R_{slow} + R_{fast} - R_{OLW}, \quad (1)$$

where  $R_{forcing}$  is the radiation due to (external) forcings, e.g. the radiation received from the sun  $R_{ins}$  and the forcing  $R_{CO_2}$  due to the greenhouse effect of atmospheric  $CO_2$ . The fluxes  $R_{slow}$  and  $R_{fast}$  are contributions to the radiative balance due to slow and fast processes in the climate system, respectively. Slow means here, that the process evolves slower than the forcing time scale. For example in the case of anthropogenic forcing the forcing time scale is several decades, while on this time scale the slow processes have hardly changed in the climate system. Slow processes are typically the land-ice albedo feedback ( $R_{LI}$ ) or vegetation changes ( $R_{VG}$ ), while typical fast processes are the sea-ice albedo feedback ( $R_{SI}$ ) or the water vapour feedback ( $R_{WV}$ ). Note however, that the separation into slow and fast processes is not unique, as there may be processes in the system that evolve on time scales similar to the forcing time scale (e.g. ocean-atmosphere heat exchange) and processes can drastically change their time scale depending on the background climate. Indeed, it can be useful to view temperature  $T$  as feeding back on atmospheric  $CO_2$  [Scheffer et al., 2006]. In this case  $R_{CO_2}$  contributes not only to  $R_{forcing}$ , but also to  $R_{slow}$  and  $R_{fast}$ . Finally,  $R_{OLW} = -\varepsilon\sigma_B T^4$  is the outgoing longwave radiation determined by the Stefan-Boltzmann law (with  $\sigma_B$  the Stefan-Boltzmann constant and  $\varepsilon$  the emissivity of the atmosphere).

Consider two forcings  $R_{forcing,1}$  and  $R_{forcing,2}$  leading to equilibrium temperatures  $T_1$  and  $T_2 = T_1 + \Delta T$  and assuming no feedbacks in the climate system. The climate sensitivity  $S$  is given by the Planck sensitivity  $S_0$ :

$$S_0 = \frac{T_2 - T_1}{R_{forcing,2} - R_{forcing,1}}, \quad (2)$$

which in the limit of small differences (i.e. similar climate states) can be expressed as

$$\begin{aligned} S_0 &= \frac{dT}{dR_{forcing}} = \frac{dT}{dR_{OLW}} = \left( \frac{dR_{OLW}}{dT} \right)^{-1}, \\ S_0(T_1) &= \left( \frac{dR_{OLW}}{dT} \right)^{-1} \Big|_{T=T_1} = (-4\varepsilon\sigma_B T_1^3)^{-1} \simeq 0.3 \text{ K (W m}^{-2}\text{)}^{-1}. \end{aligned} \quad (3)$$

Here, we have assumed the state 1 is the preindustrial climate with a global mean temperature  $T_{g,1} = 286.5 \text{ K}$  and an atmospheric emissivity  $\varepsilon = 0.6$ . In case of no feedbacks in the system, the change in radiative forcing is purely balanced by the outgoing longwave

radiation  $R_{OLW}$  (equation 1). Moreover,  $R_{OLW}$  depends only weakly and in a smooth way on the global mean temperature  $T$  such that the slope is relatively well approximated by differences between climate states.

## 1.2 Measure constraints to climate sensitivity

With feedbacks and intrinsic variability in the climate system, the initial temperature response can be modified and consequently, the observed climate sensitivity will be different from  $S_0$ . As the equilibrium assumption is only valid for those processes faster than the forcing time scale, the slow feedback processes (which are not in equilibrium) are considered forcings when studying data from distant times in the past. For example, the different amount of land ice in past climate states needs to be considered when comparing palaeo climate sensitivity to the model-derived present day climate sensitivity, for details see Rohling et al. [2012]. The climate sensitivity is again given by the ratio of the temperature change versus the radiative forcing change (including slow feedbacks):

$$S = \frac{\Delta T}{\Delta R_{forcing} + \Delta R_{slow}} \approx \frac{dT}{d(R_{forcing} + R_{slow})}. \quad (4)$$

In the (hypothetical) case that all slow processes are known and quantified and that a time-scale separation between slow and fast processes exists, the ECS will be equal to  $S_{[A,B,...]}$ . Considering a climate sensitivity involving only  $\text{CO}_2$  and land ice-albedo feedback as forcing  $R_{[CO_2,LI]}$ , we can estimate the specific climate sensitivity to a change in  $\text{CO}_2$  as the ratio of changes

$$S_{[CO_2,LI]} = \frac{\Delta T}{\Delta R_{[CO_2,LI]}}. \quad (5)$$

The use of the specific climate sensitivity is that it can give a linear prediction

$$T' = T + S_{[CO_2,LI]} \Delta R_{[CO_2,LI]}. \quad (6)$$

for the  $T' = T + \Delta T$  that results from a  $\text{CO}_2$  induced  $\Delta R_{[CO_2,LI]}$ . However, it is not clear when (5) will be defined, and if it is, whether it depends on the nature of the changes  $\Delta R$  that are considered. On the one hand,  $\Delta R$  should be small to make a linear prediction plausible. On the other hand, taking climate states where  $\Delta R$  is large is more likely to give values in (5) that are insensitive to measurement errors. Nonetheless, the quotient (5) is still a useful way to characterise climate states and how they are related to each other, even if we do not expect the linear prediction (6) to be applicable except on some mean way.

Taking a step back from the ratio (5), let us assume that there is an attractor for the climate system that is not simply equilibrium, but nonetheless stationary (this includes the possibility of a climate that is turbulent and/or that responds in a chaotic way to stationary, for example quasi-periodic, astronomical forcing). Then we expect there to be a stationary measure  $\mu$  of points in the  $(T, R_{[CO_2,LI]})$ -plane according to how often they are visited over asymptotically long times, i.e. we assume that

$$\mu(A) := \lim_{t' \rightarrow \infty} \frac{1}{t'} \ell \left( \{0 < s < t' : (T(t+s), R_{[CO_2,LI]}(t+s)) \in A\} \right). \quad (7)$$

is independent of  $t$  and typical initial condition, where  $\ell(B)$  is the length of the set  $B \subset \mathbb{R}$ : see Figure 1a. Such a measure  $\mu$  will be a projection of a natural measure for the dynamics onto the two observables  $(T, R_{[CO_2, LI]})$ , and can be viewed as a distribution (probability density) of associations between  $T$  and  $R_{[CO_2, LI]}$ . Viewed as a non-autonomous system, this distribution can be thought of as a projection of a non-autonomous invariant measure on a climate attractor [Chekroun et al., 2011] onto these observables. For such a “climate attractor”, we can also consider an instantaneous perturbation to the system under the assumption that the perturbation does not move us out of the basin of the attractor so that any response has an initial phase of decay back to the attractor followed by continued motion on the attractor. Figure 1b illustrates this schematically.

However, there are other approaches to produce relevant measures. For example, Figure 1c starts with a localised (say Gaussian) distribution  $\mu_0$  centred on an initial reference state at some time  $t_{ref}$ , with variance that quantifies measurement errors, and propagate this forwards to time  $t_{ref} + \delta$  for some  $\delta > 0$ . The initial distribution will spread to give a localised measure  $\mu_\delta$  that gives a distribution of possible sensitivities via (5). We can use this to approximate the distribution of responses  $\mu'_\delta$  after time  $\delta$  to an instantaneous perturbation as shown in Figure 1d. The distribution of sensitivities will hence potentially depend on the timescale  $\delta$  of interest and the initial time  $t_{ref}$  and the size, nature and timescale of decay of any instantaneous perturbation. In the large  $\delta$  limit, and assuming a strongly chaotic attractor we expect  $\mu_\delta$  to approach the stationary measure  $\mu$ , though in the presence of time-dependent forcing it is possible that  $\mu_\delta$  may depend nontrivially on  $\delta$  even for arbitrarily large  $\delta$ .

In any of these settings, we can think of climate sensitivity as a distribution that is a local property of a measure. Note that the ratio (5) will only be a single number (that may vary with climate state) if  $T$  is a (smooth) function of  $R_{[CO_2, LI]}$ : in this case the distribution of (5) approaches a delta function centred at  $dT/dR$ .

## 2 Climate sensitivity for a conceptual climate model

The conceptual model of the climate system of Gildor and Tziperman [2001], Gildor et al. [2002] has been shown to simulate the glacial-interglacial transitions; the model equations are given in appendix A. In this model, the atmosphere is represented by 4 meridional boxes while the ocean component consists of two layers of 4 meridional boxes each. The model couples land ice, sea ice and carbon-cycle effects, such that the atmospheric  $CO_2$  concentration is a dynamic variable in the model. The model contains one dynamic fast feedback, namely the sea ice-albedo feedback evolving on (sub-)decadal time scales, and one slow feedback, the land ice-albedo feedback, which evolves on the order of millennial time scales. On the decades-to-century time scale the model includes an additional process in the radiative balance due to heat exchange between ocean and atmosphere. All other fast feedbacks (water vapor, clouds, aerosols, lapse rate) are represented by a fixed temperature response to the radiative forcing in the system. Orbital forcing is included in the model through varying incoming solar radiation averaged over each atmospheric box on seasonal

and orbital time scales and modulating the Northern Hemisphere land ice ablation term by the (northern polar box averaged) summer insolation on orbital time scales [Gildor and Tziperman, 2000].

The full model system contains, strictly speaking one other feedback process, which deserves further discussion, namely the atmospheric  $\text{CO}_2$ -concentration itself. While the dynamic  $\text{CO}_2$  is not essential for generating the glacial-interglacial cycles in the model, it feeds back on their amplitude; during cold periods when land ice is growing, reduced vertical mixing in the Southern Ocean and extended Southern Ocean sea ice cover leads to reduced atmospheric  $\text{CO}_2$  [Gildor et al., 2002]. The exchange of  $\text{CO}_2$  between ocean and atmosphere is fast (on time scales of 10 years), however, the vertical mixing of surface-to-deep water masses in the Southern Ocean is affected by the temperature of the North Atlantic deep water, which evolves on slower time scales. The associated feedback process therefore acts on various time scales. When determining climate sensitivity,  $\text{CO}_2$  is, however, generally assumed to be a forcing. Here, it is important, to keep in mind that it also can be viewed as a feedback, not only in this model, but also in the real climate system.

## 2.1 Glacial-interglacial cycles as relaxation oscillations

We analyse a simulation with the climate model including prognostic  $p\text{CO}_2$  and Milankovitch forcing. The simulation is started 500 kyr ago from initial conditions that are assumed to be close to the attractor. It is run up until the present day. The simulated glacial-interglacial cycles show a peak-to-peak global mean temperature difference of up to 4 K (Fig. 2a). Corresponding  $\text{CO}_2$  differences are about 75 ppmv which are here completely generated by the effect of the solubility pump in the ocean. In this model the fast sea ice feedback is responsible for the abrupt glacial-interglacial variations — the so-called sea ice switch mechanism as suggested by Gildor and Tziperman [2001].

The sea ice switch mechanism generates the glacial cycles in the model as self sustained relaxation oscillations because the ice volume thresholds for switching sea ice cover ‘on’ and ‘off’ differ [Crucifix, 2012] (see Fig. 3). When the land ice volume slowly grows (accumulation exceeds ablation), the atmospheric and surface ocean temperature decrease due to increasing albedo of the planet. Once the polar surface temperature has reached a critical value cold enough to form sea ice, the polar box is rapidly covered with sea ice, which further reduces the atmospheric temperature through the ice-albedo feedback and prevents evaporation from the polar ocean box (Fig. 2b). In addition, atmospheric moisture content is reduced due to colder temperatures, which leads to decreasing land ice volume (accumulation is smaller than ablation, Fig. 2c). Temperature starts rising again both due to smaller albedo and because the ocean warms below the insulating sea-ice cover until it is warm enough to melt the polar sea ice, Fig. 2d). At this point the global temperature quickly rises, moisture content in the atmosphere increases and the land ice starts growing again (accumulation becomes larger than ablation). In this model, Milankovitch forcing is not necessary to generate the glacial-interglacial cycles in the model, but it modifies them and makes them more irregular. Although there is some degree of synchronisation of the glaciation and deglaciations to the orbital forcing, the relation between land ice and global mean solar radiation is not

trivial (Fig. 3d). Milankovitch forcing mainly modulates the (otherwise constant) ablation of the northern hemisphere land ice, and therefore, while the land ice is growing and ocean temperatures decreasing in some (slightly warmer) periods land ice accumulation becomes smaller than ablation and the ice growth and ocean cooling is reversed for a while (Fig. 2c).

## 2.2 Equilibrium climate sensitivity from short runs

Following the usual procedure in climate models, the model’s ECS can be determined from short simulations (100-200 years long), where the  $\text{CO}_2$ -concentration is either held constant or doubled within the first 30 years and held fixed afterwards. Note that in these simulations the biogeochemistry module, which dynamically determines atmospheric  $\text{CO}_2$  is switched off. More specifically, we compare the end state of a simulation with constant  $p\text{CO}_2^0$  with the end state of a simulation where  $p\text{CO}_2$  is changing in time according to

$$p\text{CO}_2(t) = p\text{CO}_2^0 + p\text{CO}_2^0 \tanh\left(\frac{t}{\tau_f}\right), \quad (8)$$

where  $\tau_f = 10$  years. The last 10 years of each simulation are averaged and used to determine the climate state. The contributions to the radiative balance of the different components such as insolation  $R_{ins}$ , atmospheric  $\text{CO}_2$   $R_{[\text{CO}_2]}$ , land ice distribution  $R_{[LI]}$  and sea ice  $R_{[SI]}$  can be explicitly calculated from the model equations (see appendix B). The climate sensitivity  $S_{2\times\text{CO}_2\text{exp}}$  estimated by

$$S_{2\times\text{CO}_2\text{exp}} = \frac{\bar{T}(2 \times p\text{CO}_2^0) - \bar{T}(p\text{CO}_2^0)}{\bar{R}_{[\text{CO}_2]}(2 \times p\text{CO}_2^0) - \bar{R}_{[\text{CO}_2]}(p\text{CO}_2^0)}, \quad (9)$$

where the overbar denotes a time-average (here 10 years). The model used here contains dynamic land ice, and the land ice-albedo feedback is the only slow feedback process affecting climate sensitivity. Therefore, the model’s ECS should be equal to the specific climate sensitivity  $S_{[\text{CO}_2, LI]}$  (eq. 5). On the short time scale of 200 years, the radiative contribution from the land-ice albedo feedback, however, hardly changes ( $\Delta R_{[LI]} \approx 0$ ) and therefore the calculated  $S_{2\times\text{CO}_2\text{exp}}$  represents a good approximation of the equilibrium climate sensitivity within this model. We determine  $S_{2\times\text{CO}_2\text{exp}}$  for 250 different background climate states along the 500 kyr time series shown in Fig. 2a (one initial condition every 2000 years). The initial  $\text{CO}_2$  concentration  $p\text{CO}_2^0$  in these simulations varies between 210 – 290 ppm, while the background global mean temperature varies between 10.8 – 14.9°C (Fig. 4a,c).

In Fig. 4e the distribution of the global mean temperature at the end of the experiments with doubled  $\text{CO}_2$  concentration is shown. Not only the mean of this distribution is shifted towards higher temperatures but also the distribution is significantly narrower than the initial temperature distribution (Fig. 4c) indicating the higher sensitivity for colder climates in this model. The distribution of the temperature and radiative forcing difference as well as the climate sensitivity  $S_{2\times\text{CO}_2\text{exp}}$  determined from these short model simulations is shown in Fig. 4b, d, f, respectively. In both the temperature change and the climate sensitivity mainly three different values occur, indicating a distinct dependence on the background



climate. The highest values of  $S_{2 \times CO_2 exp}$  occur for the coldest climates, while the lower values are associated with intermediate to warm global mean temperatures (Fig. 5a). The separation of two regimes becomes even more evident in Fig. 5b, where  $S_{2 \times CO_2 exp}$  is shown against the Northern Hemisphere sea ice cover: In cold climates more sea ice means a higher sensitivity (because more ice is available to melt), while the climate states without sea ice have a (still variable) lower sensitivity to CO<sub>2</sub>-doubling [von der Heydt et al., 2014].

The lower values of  $S_{2 \times CO_2 exp}$  occur during phases without sea-ice and separate into two main peaks (Fig. 4f). This separation suggests an additional state dependence and occurs because of the Milankovitch forcing. Without Milankovitch forcing, the sea-ice free phases in a glacial-interglacial cycle of the model are characterised by strictly growing land ice and cooling of the polar surface ocean. With Milankovitch forcing, not only the insolation varies on orbital time scales, but also the (otherwise constant) ablation in the land ice model is modulated with the Northern Hemisphere summer insolation. Therefore, the land ice mass balance can become negative (ablation larger than accumulation) during these phases of otherwise growing land ice (see Fig. 5c,d). If CO<sub>2</sub> is doubled in such a situation the warming due to CO<sub>2</sub> seems to be smaller.

## 2.3 Climate sensitivity for perturbed model climates

If we consider climate sensitivity as a local property of the natural ergodic measure on the climate attractor as illustrated in Fig. 1, we need to explore the set of points in the  $(T, R_{[CO_2, LI]})$ -plane that the model visits over the glacial-interglacial cycles and how an initial distribution  $\mu_0$  evolves over a certain time scale  $\delta$ . As shown in Fig. 1c,d the distribution of sensitivities can be found by perturbing the system instantaneously, assuming that the perturbation is not too large and the system returns to the same attractor after a transient. Note, however, that this approach requires a different type of perturbation than what has been applied in the previous section as the standard procedure in climate models; in the previous section we considered a prescribed (non-dynamic) CO<sub>2</sub>-doubling as a perturbation, where by switching off the dynamic biogeochemistry module the attractor of the model changes.

In this section, we derive the model's ECS in response to a perturbation to the initial atmospheric CO<sub>2</sub> in the fully coupled model (thus including a dynamic carbon cycle), and evaluating the temperature response to this initial perturbation at different times (following the approach illustrated in Fig. 1d). Starting from the same 250 initial conditions as in the previous section, the model is integrated for 500 years to give control runs of temperature  $T^{cntrl(i)}(t)$  and radiative forcing time series  $R_{[CO_2]}^{cntrl(i)}(t) + R_{[LI]}^{cntrl(i)}(t)$ , respectively, where the index  $i = 1, \dots, 250$  denotes the initial condition. A second set of simulations is performed, where the initial value of the CO<sub>2</sub> is doubled and then the model is integrated for 500 years, giving  $T^{pert(i)}(t)$  and  $R_{[CO_2]}^{pert(i)}(t) + R_{[LI]}^{pert(i)}(t)$ . A (time-dependent) climate sensitivity is then determined from

$$S_{perturb}^{(i)}(t) = \frac{\Delta T^{(i)}(t)}{\Delta R^{(i)}(t)} = \frac{T^{pert(i)}(t) - T^{cntrl(i)}(t)}{R_{[CO_2]}^{pert(i)}(t) + R_{[LI]}^{pert(i)}(t) - R_{[CO_2]}^{cntrl(i)}(t) - R_{[LI]}^{cntrl(i)}(t)} \quad (10)$$

In Fig. 6 time series of  $\text{CO}_2$ , temperature, Northern Hemisphere sea ice cover, the ocean meridional overturning circulation and  $S_{\text{perturb}}$  are shown for a few of the ensemble members (both control and perturbed experiments). In this case, the *equilibrium* is more difficult to specify; there is not only a separation into fast and slow processes determining the temperature in the model, but also the  $\text{CO}_2$  evolves dynamically over time. The initial doubling of  $\text{CO}_2$  leads to a (fast) temperature response after about 50-100 years, however, at that time, the  $\text{CO}_2$  has already decreased, such that beyond about 100 years the temperature starts to slowly approach an (intermediate) equilibrium value. The fastest response to the doubled  $\text{CO}_2$  is the increased atmosphere-ocean  $\text{CO}_2$ -flux, which is linearly related to the atmosphere-ocean  $\text{CO}_2$ -difference with a time scale of  $\sim 10$  years [Gildor et al., 2002] (Fig. 6a). Similarly fast is the sea ice response in those cases where sea ice is present (Fig. 6c). The strength of the ocean meridional overturning circulation (MOC) also responds to increased  $\text{CO}_2$ , although somewhat slower (Fig. 6d). In particular, this response occurs in small steps after 100-200 years in those simulations that originally had sea ice. This is because the MOC strength depends on the meridional temperature gradient of the surface ocean boxes, which changes only after the sea ice has melted.

The climate sensitivity  $S_{\text{perturb}}$  depends on time, however, it seems to approach some *fast-process-equilibrium* (Figs. 6e) after 200-500 years, still before the land ice volume starts to considerably change. The distribution of  $S_{\text{perturb}}$  evaluated at the last 10 years of the 500 year long simulations is shown in Fig. 7a and is almost identical to the distribution evaluated 100 or 200 years after the perturbation (not shown). As before, the climate sensitivity  $S_{\text{perturb}}$  is higher for those climate states that had sea ice, however, their values are higher and much broader distributed than in the simulations with prescribed  $\text{CO}_2$  (compare Fig. 7a, b with Fig. 4f, 5b). Also the initial conditions without sea ice lead to slightly varying  $S_{\text{perturb}}$  values depending on land-ice growth or decrease (Fig. 7c, d), however, this variation is much less pronounced than in the simulations with prescribed  $\text{CO}_2$  (Fig. 5c, d).

### 3 Sensitivity for unperturbed climates from the palaeo record

In the previous section, we have determined the climate sensitivity following two different approaches, where a perturbation to the atmospheric  $\text{CO}_2$  is applied with or without dynamic  $\text{CO}_2$ . In the case of a past climate record, we have only one realisation of the temporal evolution of the climate in the form of a time series, which may visit different points on the attractor. Perturbations away from the attractor as in the previous section are not applied. The climate sensitivity that is estimated from such records, is, therefore, (linearly) connecting different points (or climate states) on the attractor (as illustrated in Fig. 1c).

The issue with defining an 'equilibrium' remains, however, and is only well-defined if a sufficient separation between *slow* and *fast* time scales exists. In long palaeo-records, the temporal resolution is sometimes quite low and in many cases each time point in a time series may be considered averaged conditions [Köhler et al., 2010]. In the presence

of climate variations on millennial time scales such as the large, rapid but intermittent changes during Dansgaard-Oeschger events which are believed to be caused by nonlinear processes in the climate system [Schulz, 2002, Ganopolski and Rahmstorf, 2002, Ditlevsen and Ditlevsen, 2009] the average-assumption may not be valid, and points in time may rather reflect snapshots or short-time averages. Even the glacial-interglacial cycles might be an oscillation between different almost stable equilibria - as in the present simple climate model - caused by nonlinear feedbacks within the system itself. In this case, comparing different climate states across the oscillation cycle might also violate the equilibrium assumption.

### 3.1 The temperature - radiative forcing relationship

Defining climate sensitivity as a local property of the measure on the climate attractor, we need to consider the relation between temperature  $T$  and radiative forcing due to  $\text{CO}_2$  and land ice (the only slow process in the climate model) as shown in Fig. 8 in terms of a probability density of  $T$ ,  $R$  combinations. In the special case of this relation being a linear function  $T(R)$ , the climate sensitivity is given by the slope of this line and constant for all climate states. However, in the climate model and most likely in the real climate system as well, the climate sensitivity seems to be strongly state dependent [von der Heydt et al., 2014, Köhler et al., 2015], which allows only the definition of a local climate sensitivity (around a reference or background climate state). Indeed, in Fig. 8 there are regimes where the  $T - R$  relation is close to a (linear) function, but particularly in the transition region from glacial to interglacial states the slope  $dT/dR$  is less well defined or even negative. Moreover, the relation  $T - R$  may not be a (smooth) function leading to a distribution of slopes  $\frac{dT}{dR}$  for each background climate.

As a first approximation, we can estimate  $S_{local}$  as the slope of the relation between  $T$  and  $R_{[CO_2, LI]} = R_{[CO_2]} + R_{[LI]}$  (Fig. 8b) by a linear regression on the warm and cold parts of the data, giving  $S_{local}(warm) = 0.45\text{K (W m}^{-2}\text{)}^{-1}$ , and  $S_{local}(cold) = 0.54\text{K (W m}^{-2}\text{)}^{-1}$ , respectively. In the regression all points with  $T \leq 12^\circ\text{C}$  are considered for  $S_{local}(cold)$  and points with  $12,5^\circ\text{C} \leq T \leq 14,5^\circ\text{C}$  for  $S_{local}(warm)$ , respectively. For the warm part of the data (climate without sea ice), where the linear relation is a reasonable assumption,  $S_{local}(warm)$  roughly agrees with the mean of the sensitivity distribution for the perturbed model experiments  $S_{perturb}$  (Fig. 7a). For the cold part of the data (climate with sea ice), the linear assumption clearly is less appropriate, and therefore  $S_{local}(cold)$  considerably underestimates  $S_{perturb}$  for the cold climates. Interestingly,  $S_{local}$  is everywhere larger than  $S_{2 \times CO_2 exp}$  derived following the classical climate model approach with prescribed (non-dynamic)  $\text{CO}_2$  (Fig. 4f).

This approach of (local) linear regressions has been applied to palaeo data of the last 800 kyr in von der Heydt et al. [2014] to show that the climate sensitivity is indeed dependent on the background climate state. The state dependence becomes even more evident when analysing palaeo data of various sources reaching back in time as far as 5 million years as done in Köhler et al. [2015]. Instead of using linear regression methods on (relatively arbitrary chosen) parts of the data Köhler et al. [2015] have chosen to fit non-linear functions to the complete data set. This adds further complications to the analysis as the type of function is impossible to derive from first principles. As discussed above, there may indeed not exist

such a functional relationship. Moreover, palaeo data become increasingly more uncertain as they reach further back in time, which makes it difficult to decide whether a functional fit is inadequate because of the wrong function (linear or nonlinear) or because of data-uncertainties [Martinez-Boti et al., 2015, Köhler et al., 2015]. While this approach is valuable for detecting any state dependence of the climate sensitivity in a given data set, it is less appropriate for determining actual values, in particular if the present climate state – where we are most interested in the climate sensitivity – lies at one end of the covered climate regimes, see Köhler et al. [2015].

### 3.2 Comparing past climate states in time

In palaeo climate studies aiming at deriving the climate sensitivity very often different climate states are compared to each other in time. This corresponds to comparing different climate states on the climate attractor (or the projection of the attractor on the  $T - R$  plane) to each other. Again, if the  $T(R)$  relation would be linear, a constant climate sensitivity could be unambiguously derived, however, when this is not the case, we must carefully consider the distance in time between the two climate states.

The simplest way to determine climate sensitivity from past climate records is to compare each climate state in time to the *preindustrial* climate at time  $t_{ref} \equiv 0$ :

$$S_{[CO_2,LI]}(\delta) = \frac{T(t_{ref} + \delta) - T(t_{ref})}{R_{[CO_2]}(t_{ref} + \delta) + R_{[LI]}(t_{ref} + \delta) - R_{[CO_2]}(t_{ref}) + R_{[LI]}(t_{ref})} \quad (11)$$

This time series derived from the model glacial-interglacial time series is shown in Fig. 9 and varies considerably over time. During phases with little or no sea ice, the sensitivity is between  $0.4\text{--}0.5 \text{ K (W m}^{-2}\text{)}^{-1}$ , while it increases to  $1\text{--}1.5 \text{ K (W m}^{-2}\text{)}^{-1}$  during phases with sea ice present. At two instances very large or even negative values can occur; (i) during the interglacial phases that are similar to the reference climate (here taken as  $t_{ref} = 0$ ) and (ii) during the fast transitions, where the sea-ice rapidly melts. The former (i) happens because a climate with very similar radiative forcing as the reference climate is compared, i.e. division by almost zero in equation 11, and has been noted in palaeo data approaches [Rohling et al., 2012]. It is also reflected in Figs. 10c where the values of  $S_{[CO_2,LI]}$  are shown against sea ice cover. Considering the glacial-interglacial variations of the last 800 kyr, this is unfortunate, because the climate is mostly colder than the preindustrial climate, while we are interested in the climate sensitivity of the warm climates. The large values of the climate sensitivity at sea ice melt phases (ii) occur for a different reason; in this case, climate states are compared to the (interglacial) reference climate that lie in the glacial regime of the phase space (see Fig. 8b), independent of whether it would be possible to reach the interglacial reference climate in the underlying short time scale of a few hundred years. The distribution of  $S_{[CO_2,LI]}(\delta)$  (see Fig. 11c), therefore shows two maxima, with one approximating the climate sensitivity  $S_{perturb}$  during warm climate states (see Fig. 11c), while the higher values of  $S_{[CO_2,LI]}(\delta)$  during sea ice phases considerably overestimate  $S_{perturb}$  (see Fig. 11a). Note, that these higher values are not exclusively from sea ice phases, but also contain entries from interglacial phases that are very similar to the reference climate.

One way to circumvent the divergence-problem (i) is to choose different reference times (or climate states) for determining climate sensitivity from past climate time series. We expand the above described method to determine palaeo climate sensitivity (Eq. (11)) by considering all possible reference times  $t_{ref}$  in the time series and delays  $\delta = t - t_{ref}$  with respect to the reference time. We restrict the delay to less than 1/4 of the average period of the glacial-interglacial cycles, i.e.,  $\delta = 0 - \pm 25$  kyr, and calculate  $S_{[CO_2, LI]}(\delta, t_{ref})$  following equation 11. The result is shown in Fig. 10a, where the black shading indicates very large ( $\geq 3$  K (W m<sup>-2</sup>)<sup>-1</sup>) positive and all negative values, respectively. In Fig. 10b the same climate sensitivity is shown against sea ice cover. For the climate states without sea ice, still high climate sensitivities occur, mostly from larger delays (smaller yellow/blue symbols), which results in a broader distribution of  $S_{[CO_2, LI]}(\delta, t_{ref})$  (see Fig. 11b) as compared to  $S_{perturb}$  (see Fig. 11a). However, by restricting the delay  $\delta$  to less than 1/4 of the glacial-interglacial period comparison of very similar climate states is largely avoided. Also for the climate states with sea ice a wide range of  $S_{[CO_2, LI]}(\delta, t_{ref})$  values occurs (see Fig. 10b, Fig. 11b), but when considering smaller delays (green and brown symbols in Fig. 10b) frequently occurring values lie between 0.6 K (W m<sup>-2</sup>)<sup>-1</sup> and 1 K (W m<sup>-2</sup>)<sup>-1</sup> as observed for  $S_{perturb}$ . The climate sensitivity during cold climates is still overestimated, because the cross-comparison between different climate regimes (sea ice and non-sea ice, ii) is not eliminated by this approach.

The problem of cross-comparison between different climate regimes (ii) should be overcome by considering only small delay times  $\delta$ . In Fig. 10d  $S_{[CO_2, LI]}(t_{ref})$  for a constant (small) delay of  $\delta = 500$  yr is shown against sea ice cover. Indeed, the higher values for the climate sensitivity are mostly eliminated by this approach, however, the climate sensitivity during sea ice phases is now frequently underestimating  $S_{perturb}$  (see also Fig. 11d). Here, a time-scale problem in the different approaches to climate sensitivity becomes apparent; when perturbing the climate system away from the attractor as done for calculating  $S_{perturb}$  the sea ice melts within 10 years in all climate states where sea ice is present, and because then the sea ice-albedo feedback is strong, a large value for  $S_{perturb}$  is attained. On the other hand, when no perturbations are applied, but the time series living on the attractor of the climate model is used to determine  $S_{[CO_2, LI]}(t_{ref})$ , in most cases the sea ice changes only little in the delay time of 500 years (because the sea ice phases are 10-20 kyr long), which appears as a rather weak sea ice-albedo feedback.

### 3.3 Conclusions

Clearly, we cannot get reliable quantitative conclusions about the distribution of ECS from a low order conceptual model such as that used in this study. Many important processes in the climate system (such as the impact of  $T$  on cloud formation) are absent from this model, and the model was constructed with the aim of explaining ice age pacing rather than the link between  $T$  and CO<sub>2</sub> [Gildor and Tziperman, 2001, Gildor et al., 2002]. Even those processes that are included are open to question; for example, the sea ice cover changes in the model are about 1.5 times larger than suggested by proxy data [Köhler et al., 2010], while Northern Hemisphere land ice cover changes are smaller (Fig. 2b). Moreover, the climate sensitivity derived from the model is higher during glacial periods, because the (only model-included)

fast sea ice-albedo feedback is stronger in those phases. Proxy data suggest, however, higher climate sensitivity during warm periods [von der Heydt et al., 2014, Köhler et al., 2015], most likely because a combination of other fast feedbacks (such as water vapour, cloud feedbacks, etc.) may be stronger during warm climates.

Nonetheless, even for this model, the presence of variability on the attractor on a number of timescales means there are clear and non-trivial distributions of sensitivities, even for unperturbed climates. The distribution of sensitivities depends strongly on the background state as well as on the timescale considered. This suggests that it could be useful to think of the unperturbed climate sensitivity as a local property of the “climate attractor”. For a perturbed system (we have considered instantaneously doubled  $\text{CO}_2$ ) this is still useful once an initial transient has decayed. This transient will depend in particular on ocean heat uptake, though also on carbon cycle and biosphere processes that act on time scales roughly equivalent with the forcing time scale. If the climate system has more than one attractor, the perturbed system may clearly evolve to a completely different set of states than the original attractor – a situation that did not occur in the climate model used here. In less extreme cases, there may still be very long transients for some perturbations associated parts of the climate system that are associated with slow feedbacks.

Such perturbations (illustrated in Fig. 1b,d) are not normally applied in climate models used for climate predictions [IPCC, 2013], where climate sensitivity is derived from model simulations considering prescribed, non-dynamic atmospheric  $\text{CO}_2$ . In our conceptual model, we have derived climate sensitivities from both types of perturbations and find that the classical climate model approach (section 2.2, Fig. 4f) leads to significantly lower values of the climate sensitivity than the perturbations away from the attractor with dynamic  $\text{CO}_2$  (section 2.3, Fig. 11a). This emphasises the importance of including dynamic carbon cycle processes into climate prediction models. Moreover, it supports the idea that the real observed climate response may indeed be larger than the model predicted one, because those models never will include all feedback processes in the climate system.

Perturbations as described above can be applied in climate models, but not in observed (or reconstructed) past climate changes. When we want to infer climate sensitivity relevant for future climate evolution from climate changes that have occurred in the past and can be reconstructed from palaeoclimate records, we need to make sure that the distribution of responses  $\mu_\delta$  as derived from the palaeoclimate record (see Fig. 1c) is indeed approximating the distribution of responses  $\mu'_\delta$  after a perturbation (see Figs. 1d and 11a). From the model time series of the glacial-interglacial cycles (or a palaeorecord), it is, however, not so easy to find the correct distribution of responses  $\mu_\delta$ ; considering all possible combinations of climate states, largely irrespective of how far in time they are separated,  $S_{[\text{CO}_2, \text{LI}]}(\delta, t_{\text{ref}})$  shown in Fig. 11b leads indeed to a distribution similar to  $S_{\text{perturb}}$ , but the cross-comparison between different climate regimes (that in fact can never be reached within short time scales  $\delta$ ) leads to differences between the two distributions. Different subsections of the distribution  $\mu_\delta$  are shown in Figs. 11c,d for considering a fixed initial distribution  $\mu_0$  (or reference time  $t_{\text{ref}}$ ) or a fixed time scale (or delay)  $\delta$ , respectively.

Considering only one fixed reference climate or initial distribution leads to many unre-

alistically large values of the climate sensitivity for every climate state in the past that is similar to that reference climate as shown in Fig. 11c. When the reference climate is chosen as the present-day or preindustrial climate this is problematic because in fact all data from climate states similar to the present one need to be excluded from the analysis, while at the same time these are the climates that we are most interested in. Moreover, having in mind the palaeoclimate record of the last 1 million years, where more and more reliable (ice-core record) data exist than before that time, excluding the similar-to-present climate states from the analysis means that for determining the climate response we consider mostly colder-than-present climates and miss information on warmer-than-present climates. On the other hand, considering only small delays  $\delta$  for all possible reference climates in the record (Fig. 11d) leads to a number of climate sensitivity values that seem to be smaller than those derived from the perturbed climate attractor (Fig. 11a), because such large perturbations on  $\text{CO}_2$  (where all sea ice melts quickly) did not occur within the long model time series.

Improving our understanding of the active feedback processes and exploring the 'climate attractor' in warmer-than-present climates in the past is thus of particular importance. However, these climate states lie mostly far back in time, beyond the ice-core period, such that proxy records of these times become increasingly uncertain. Model studies with potentially dynamic carbon cycle can be very helpful in this respect.

# A Model equations

## A.1 Ocean and sea ice

The ocean consists of 2 layers of 4 meridionally oriented boxes, where the polar boxes extend from  $45^\circ$  to the pole and the equatorial boxes from the equator to  $45^\circ$ , with meridional lengths  $L_1, L_2, L_3, L_4$  the same as the atmospheric boxes. All tracers such as temperature  $T$ , salt  $S$  and biogeochemical variables are averaged over the two equatorial boxes, such that in fact the dynamics is determined by only three meridional boxes. The two vertical layers have thicknesses  $D_{upper}$  and  $D_{lower}$ , respectively. The ocean model dynamics includes a simple frictional horizontal momentum balance, is hydrostatic and mass-conserving:

$$0 = -\frac{1}{\rho_0} \frac{\partial p}{\partial z} - \frac{g}{\rho_0} \rho \quad (12)$$

$$0 = -\frac{1}{\rho_0} \frac{\partial p}{\partial y} - rv \quad (13)$$

$$0 = \frac{\partial v}{\partial y} + \frac{\partial w}{\partial z} \quad (14)$$

Here,  $(y, z)$  are the meridional and vertical coordinates and  $(v, w)$  the corresponding flow velocities, respectively.  $p$  is the pressure,  $g$  the gravitational constant,  $\rho_0$  a reference density and  $r$  a friction coefficient. In each box, temperature  $T$  and salinity  $S$  determine the density via the full nonlinear equation of state as recommended by UNESCO [1981]. Temperature and salinity are determined by the following balances:

$$\frac{\partial T}{\partial t} + \frac{\partial(vT)}{\partial y} + \frac{\partial(wT)}{\partial z} = K_h \frac{\partial T}{\partial y} + K_v \frac{\partial T}{\partial z} + Q_T^{atm} + Q_T^{sea-ice} \quad (15)$$

$$\frac{\partial S}{\partial t} + \frac{\partial(vS)}{\partial y} + \frac{\partial(wS)}{\partial z} = K_h \frac{\partial S}{\partial y} + K_v \frac{\partial S}{\partial z} + Q_S^{atm} + Q_S^{sea-ice} + Q_S^{land-ice} \quad (16)$$

where  $K_h$  and  $K_v$  are horizontal and vertical diffusion coefficients, respectively. As in Gildor et al. [2002], the vertical mixing of any tracer  $tr$  (e.g., temperature, salinity or ocean  $\text{CO}_2$ ) in the southern polar box is dependent on the vertical stratification:

$$K_v^0 (\sigma_{t_{deep}} - \sigma_{t_{surface}})^{-1} (tr_{deep} - tr_{surface}), \quad (17)$$

where  $(\sigma_{t_{deep}} - \sigma_{t_{surface}}) \sim d\rho/dz$ . In addition, upper and lower bounds of 280 and 1 Sv are imposed on the vertical mixing rates  $K_v^0 (\sigma_{t_{deep}} - \sigma_{t_{surface}})^{-1}$ . Vertical mixing rates between the other surface and deep boxes are set constant, 0.25 Sv for the two equatorial boxes and 5 Sv for the northern polar box. The meridional overturning circulation is treated in the same way as in Gildor et al. [2002], with the upwelling through the southern polar box set to a fixed value of 16 Sv and the downwelling through the northern polar box determined by the meridional density gradient between the northern equatorial and polar ocean boxes.



The  $Q$  terms in the above equations are fluxes from other components of the climate model:  $Q_T^{atm}$  is the atmosphere-ocean heat flux due to sensible, latent and radiative fluxes:

$$Q_T^{atm} = \frac{\rho_0 C_{pw} D_{upper}}{\tau} (\theta - T) (f_{ow} + f_{si} \frac{\gamma}{D_{sea-ice}}), \quad (18)$$

where  $C_{pw}$  is the heat capacity of water,  $\theta$  the temperature of the atmospheric box above,  $\gamma$  the insolation effect of a layer sea ice of thickness  $D_{sea-ice}$ .  $f_{ow}$  and  $f_{si}$  are the fractions of the ocean that are open water and sea ice covered, respectively, with  $f_{ow} = 1 - f_{si}$ . The time scale  $\tau$  is chosen such that the ocean heat transport into the northern polar atmospheric box is about 2.3PW during interglacial periods as in Gildor and Tziperman [2001]. Precipitation  $P$  and evaporation  $E$  is converted into an equivalent salt flux:

$$Q_S^{atm} = -(P - E)S_0, \quad (19)$$

with  $S_0$  a reference salinity. Heat and salt fluxes due to sea ice formation or melting are formulated as:

$$Q_T^{sea-ice} = \frac{\rho_0 C_{pw} V_{ocean}}{\tau_{sea-ice}} (T^{sea-ice} - T), \quad (20)$$

$$Q_S^{sea-ice} = \frac{Q_T^{sea-ice}}{\rho_{sea-ice} L_f} S_0, \quad (21)$$

where  $V_{ocean}$  is the volume of the ocean box,  $T^{sea-ice}$  is the temperature threshold where sea ice forms,  $L_f$  is the latent heat of fusion,  $\rho_{sea-ice}$  the density of sea ice and  $\tau_{sea-ice}$  is a short time scale to ensure that the ocean temperature remains close to the freezing temperature as long as sea ice is present. Sea ice is assumed to grow in area with an initial thickness of 3 and 1.5m in the northern and southern polar boxes, respectively, until the whole box is covered. The volume of sea ice in the polar surface boxes  $V_{sea-ice}$  is given by:

$$\frac{dV_{sea-ice}}{dt} = \frac{Q_T^{sea-ice}}{\rho_{sea-ice} L_f} + P_{on-ice}. \quad (22)$$

$P_{on-ice}$  is the amount of sea ice forming due to atmospheric precipitation falling on the ocean area covered with sea ice.

## A.2 Atmosphere

The atmospheric model follows that used in Gildor et al. [2002], with 4 atmospheric boxes above the ocean boxes. The lower surface of each atmospheric box can be either land or ocean, and both can be partly covered with (land or sea) ice. The box-averaged potential temperature is calculated from the energy balance of the box, balancing incoming solar radiation (with a box albedo determined from the relative fraction of each lower surface type in the box), outgoing longwave radiation at the top of the atmosphere, air-sea heat flux and meridional atmospheric heat transport. In each atmospheric box, the temperature  $\theta$  is

determined by the difference between the heat flux at the top of the atmosphere  $F_{top}$  and at the surface  $F_{surface}$ , following the equation:

$$\frac{\partial \theta}{\partial t} = \frac{2^{R/C_p} g}{P_0 C_p} [(F_{top} - F_{surface}) + (F_{merid}^{out} - F_{merid}^{in})] \quad (23)$$

$$= \frac{2^{R/C_p} g}{P_0 C_p} [(H_{in} - H_{out} - Q_T^{atm}) + (F_{merid}^{in} - F_{merid}^{out})], \quad (24)$$

where

$$H_{in} = (1 - \alpha_{surf})(1 - \alpha_C)(1 - q_{in}^{seaice})Q_{Solar} \quad (25)$$

$$H_{out} = \left( \varepsilon - \kappa \ln \left( \frac{\text{CO}_2}{\text{CO}_{2,ref}} \right) \right) \sigma_B \theta^4, \quad (26)$$

are the incoming and outgoing radiation terms at the top of the atmosphere, respectively. ( $R$  is the gas constant for dry air,  $C_p$  is the specific heat of the atmosphere at a constant pressure,  $P_0$  a reference pressure,  $\sigma_B$  the Stefan Boltzmann constant and  $g$  the gravitational acceleration.) The incoming solar radiation  $Q_{Solar}$  for each box is assumed to vary with season and due to orbital variations as in Gildor and Tziperman [2000]. Furthermore,  $Q_{Solar}$  is reduced by a constant cloud albedo term  $\alpha_C$  and a part  $q_{in}^{seaice}$  that is directly used to melt sea ice; where sea ice exists, 15% of the incoming shortwave radiation is used to melt sea ice and does not enter the radiation balance of the atmosphere [Gildor et al., 2002].  $\alpha_{surf}$  is the surface albedo of the box and is determined by the fraction of sea ice, land ice, land surface and ocean surface in that box:

$$\alpha_{surf} = f_L(1 - f_{LI})\alpha_L + f_L f_{LI}\alpha_{LI} + f_O(1 - f_{SI})\alpha_O + f_O f_{SI}\alpha_{SI} \quad (27)$$

Here,  $f_L$ ,  $f_{LI}$ ,  $f_O$ ,  $f_{SI}$  correspond to the fraction of land, land ice, ocean and sea ice, respectively, and  $\alpha_L$ ,  $\alpha_{LI}$ ,  $\alpha_O$ ,  $\alpha_{SI}$  to the corresponding albedos of each surface type. The outgoing radiation depends on a mean emissivity of the box  $\varepsilon$  and a term depending on the atmospheric  $\text{CO}_2$  concentration. Here  $\kappa$  is chosen [Gildor et al., 2002] such that a doubling of  $\text{CO}_2$  will cause a radiative forcing of  $4 \text{ Wm}^{-2}$ .  $F_{merid}^{in} - F_{merid}^{out}$  is the net heating due to meridional heat fluxes between the atmospheric boxes. Meridional heat transport between boxes is calculated as:

$$F_{merid} = K_\theta \nabla \theta, \quad (28)$$

where the coefficient  $K_\theta$  is chosen such that the meridional heat transport between the two northern boxes is about 2.2 PW during interglacial periods [Gildor and Tziperman, 2001]. No net heat flux is assumed over land and land ice, therefore  $F_{surface}$  includes only the ocean-atmosphere heat exchange.

The meridional moisture transport  $F_{Mq}$  between the atmospheric boxes is parameterised as:

$$F_{Mq} = K_{Mq} |\nabla \theta| q, \quad (29)$$

where  $q$  is the humidity of the box. A constant relative humidity is assumed, with the saturation humidity at temperature  $\theta$  calculated from an approximate Clausius-Clayperon equation:

$$q = 0.7 \cdot A \cdot e^{B/\theta}. \quad (30)$$

Over land ice in the polar boxes, another source of precipitation is the local evaporation of that part of the ocean box that is not covered by sea ice, with flux:

$$F_q = K_q f_{ow} q. \quad (31)$$

The total precipitation in each box is then given by

$$P - E = -\nabla \cdot (F_{Mq} + F_q). \quad (32)$$

Precipitation falling over land or sea ice is assumed to turn into additional ice.

### A.3 Land ice

The equations for the land ice sheets follow those of Gildor and Tziperman [2001], with the mass balance

$$\frac{dV_{ice-sheet}}{dt} = LI_{source} - LI_{sink}. \quad (33)$$

The source term  $LI_{source}$  depends on the amount of precipitation falling over existing ice (or falling on the 0.3 poleward area of the box even if there is no glacier there):

$$LI_{source} = \frac{\max\{0.3L_{area}, LI_{area}\}}{box_{area}}(P - E), \quad (34)$$

where  $L_{area}$  is the land area in the box,  $LI_{area}$  the ice sheet area and  $box_{area}$  the total area of the box.

The ice sheet can shrink as a consequence of ablation. The ablation term is assumed a constant  $C_{LI}$  [Gildor and Tziperman, 2001] plus a modulation by the summer Milankovitch forcing [Gildor and Tziperman, 2000]:

$$LI_{sink} = C_{LI} + \gamma_{LI}(Solar_{June} - Solar_{ave, June}), \quad (35)$$

where  $Solar_{June} - Solar_{ave, June}$  is the anomaly in summer insolation in this box relative to the average over the past 1 Myr. Southern hemisphere ice sheets are assumed constant.

### A.4 Biogeochemistry

In the ocean boxes additional tracers are advected for total  $CO_2$  ( $\Sigma CO_2$ ), alkalinity ( $A_T$ ) and phosphate  $PO_4$ . These are used to calculate atmospheric  $pCO_2$ , see Gildor et al. [2002]. The equations for the three biogeochemistry variables  $Bio$  in each ocean box follow:

$$\frac{\partial Bio}{\partial t} + \frac{\partial(vBio)}{\partial y} + \frac{\partial(wBio)}{\partial z} = K_h \frac{\partial Bio}{\partial y} + K_v \frac{\partial Bio}{\partial z} + S_{Bio}, \quad (36)$$

with additional source/sink terms  $S_{Bio}$  for these variables in the surface boxes:

$$S_{\Sigma CO_2} = -R_C \times EP - RR \times EP + PV([CO_{2,a}] - [CO_{2,o}]) \quad (37)$$

$$S_{AT} = -2 \times RR \times EP + R_N \times EP \quad (38)$$

$$S_{PO_4} = -EP, \quad (39)$$

and in the deep boxes below:

$$S_{\Sigma CO_2} = R_C \times EP + RR \times EP \quad (40)$$

$$S_{AT} = 2 \times RR \times EP - R_N \times EP \quad (41)$$

$$S_{PO_4} = EP. \quad (42)$$

$EP$  and  $RR$  stand for export production and rain ratio, respectively, and  $R_C$ ,  $R_N$  for the ratio  $P : C$  and  $P : N$  in particulate organic matter, respectively.  $[CO_{2,a}]$  is the saturation concentration with regard to the partial pressure of  $CO_2$  in the atmosphere, and  $[CO_{2,o}]$  is the  $CO_2$  concentration in the ocean. The flux of  $CO_2$  between ocean and atmosphere  $F_{CO_2} = PV([CO_{2,a}] - [CO_{2,o}]) A_{openwater}$  is linearly related to the  $pCO_2$  difference between the atmosphere and the surface ocean via a constant piston velocity  $PV$ , giving a time scale of about 10 years for this gas exchange. For more details on the biogeochemistry module, see Gildor et al. [2002].

## B Climate sensitivity in the model

Climate sensitivity is determined from the energy balance of the Earth. For the conceptual model [Gildor and Tziperman, 2001], we can explicitly write the energy balance of the atmosphere and extract the different contributions to climate sensitivity. Averaged over all atmospheric boxes of the model the global mean temperature  $T = \sum_{i=1}^4 \frac{area_i}{area} \theta_i$  is determined by the difference between the heat flux at the top of the atmosphere  $F_{top}$  and at the surface  $F_{surface}$  (see previous section), where  $area_i$ , ( $i = 1, \dots, 4$ ) is the surface area of the 4 boxes and  $area$  is the total surface area of the Earth.

To access the contributions of the different forcings and feedbacks to the radiation balance, we split the global mean radiation terms into the different components due to solar radiation ( $R_{[ins]}$ ), land ice ( $R_{[LI]}$ ), sea ice ( $R_{[SI]}$ ), outgoing longwave radiation ( $R_{[OLW]}$ ),  $CO_2$  concentration ( $R_{[CO_2]}$ ) and the radiation at the Earth's surface ( $R_{[surf]}$ ):

$$\frac{\partial T}{\partial t} = \frac{2^{R/C_p} g}{P_0 C_p} [R_{[ins]} + R_{[LI]} + R_{[SI]} + R_{[OLW]} + R_{[CO_2]} + R_{[surf]}] \quad (43)$$

The different contributions to the radiation balance can be expressed as:

$$R_{[ins]} = (1 - \alpha_C)Q_{solar} \quad (44)$$

$$R_{[LI]} = R_{[ins]} \sum_i \frac{area_i}{area} (f_L^i (1 - f_{LI}^i) \alpha_L + f_L^i f_{LI}^i \alpha_{LI}) (q_{in}^{seaice} - 1) \quad (45)$$

$$R_{[SI]} = -R_{[ins]} \sum_i \frac{area_i}{area} [q_{in}^{seaice} + (1 - q_{in}^{seaice}) (f_O^i (1 - f_{SI}^i) \alpha_O + f_O^i f_{SI}^i \alpha_{SI})] \quad (46)$$

$$R_{[OLW]} = - \sum_i \frac{area_i}{area} \varepsilon_i \sigma_B \theta_i^4 \quad (47)$$

$$R_{[CO_2]} = \sum_i \frac{area_i}{area} \kappa \ln \frac{pCO_2}{pCO_{2,ref}} \sigma_B \theta_i^4 \quad (48)$$

$$R_{[surf]} = - \sum_i \frac{area_i}{area} Q_{oa}^i. \quad (49)$$

When comparing two equilibrium climate states with global mean temperatures  $T_1$  and  $T_2$  (and  $\Delta T = T_2 - T_1$ ), the radiation balance Eq.43 reads:

$$0 = \Delta R_{[ins]} + \Delta R_{[LI]} + \Delta R_{[SI]} + \Delta R_{[OLW]} + \Delta R_{[CO_2]} + \Delta R_{[surf]}. \quad (50)$$

As we consider constant solar radiation and no changes in cloud albedo,  $\Delta R_{[ins]} = 0$ , and, when we put all the forcing or slow feedbacks on the left hand side and all fast feedback processes on the right hand side, we obtain:

$$\Delta R_{[CO_2]} + \Delta R_{[LI]} = -\Delta R_{[OLW]} - \Delta R_{[SI]} - \Delta R_{[surf]}. \quad (51)$$

This finally leads to the expressions for the specific climate sensitivities

$$S_{[CO_2]} = \frac{\Delta T}{\Delta R_{[CO_2]}} = \frac{-\Delta T}{\Delta R_{[OLW]} + \Delta R_{[SI]} + \Delta R_{[surf]} + \Delta R_{[LI]}} \quad (52)$$

$$S_{[CO_2, LI]} = \frac{\Delta T}{\Delta R_{[CO_2]} + \Delta R_{[LI]}} = \frac{-\Delta T}{\Delta R_{[OLW]} + \Delta R_{[SI]} + \Delta R_{[surf]}} \quad (53)$$

$$S_{[CO_2, LI, SI]} = \frac{\Delta T}{\Delta R_{[CO_2]} + \Delta R_{[LI]} + \Delta R_{[SI]}} = \frac{-\Delta T}{\Delta R_{[OLW]} + \Delta R_{[surf]}}. \quad (54)$$

The last expression should approximate the sensitivity without feedbacks (i.e. only Planck feedback),  $S_0 = (-4\varepsilon\sigma_B T^3)^{-1} \simeq 0.3 \text{ K (W m}^{-2}\text{)}^{-1}$ . In the model there is, however, one more radiation term due to the atmosphere-ocean heat exchange ( $\Delta R_{surf}$ ), which acts on fast to intermediate time scales. Therefore,  $S_{[CO_2, LI, SI]}$  still slightly deviates from the Planck sensitivity.

## Acknowledgements

This work was carried out under the program of the Netherlands Earth System Science Centre (NESSC), financially supported by the Ministry of Education, Culture and Science (OCW)

in the Netherlands. AH thanks CliMathNet (sponsored by EPSRC) for travel support to meetings that facilitated this work. We thank the Lorentz Center in Leiden for organising a "Workshop on Climate Variability: from Data and Models to Decisions" in 2014 where this was first discussed.

## References

- T. Andrews and P. M. Forster. CO<sub>2</sub> forcing induces semi-direct effects with consequences for climate feedback interpretations. *Geophys. Res. Lett.*, 35:L04802, 2008. doi: 10.1029/2007GL032273.
- R. Caballero and M. Huber. State-dependent climate sensitivity in past warm climates and its implications for future climate projections. *Proceedings of the National Academy of Sciences*, 110:14162–14167, 2013.
- J. G. Charney. *Carbon Dioxide and Climate: A Scientific Assessment*. National Academy of Science, Washington, D.C., U.S.A, 1979.
- M. D. Chekroun, E. Simonnet, and M. Ghil. Stochastic climate dynamics: Random attractors and time-dependent invariant measures. *Physica D: Nonlinear Phenomena*, 240(21):1685–1700, 10 2011. doi: 10.1016/j.physd.2011.06.005.
- M. Crucifix. Does the Last Glacial Maximum constrain climate sensitivity? *Geophys. Res. Lett.*, 33(18):L18701, 2006. doi: 10.1029/2006GL027137.
- M. Crucifix. Oscillators and relaxation phenomena in Pleistocene climate theory. *Philosophical Transactions of the Royal Society A: Mathematical, Physical and Engineering Sciences*, 370(1962):1140–1165, 2012. doi: 10.1098/rsta.2011.0315.
- P. D. Ditlevsen and O. D. Ditlevsen. On the stochastic nature of the rapid climate shifts during the last ice age. *J. Clim.*, 22:446–457, 2009. doi: 10.1175/2008jcli2430.1.
- A. Ganopolski and S. Rahmstorf. Abrupt glacial climate change due to stochastic resonance. *Physical Review Letters*, 88(3):038501–1–4, 2002. doi: 10.1103/PhysRevLett.88.038501.
- M. Ghil. *Climate Change: Multidecadal and Beyond*, chapter A Mathematical Theory of Climate Sensitivity or, How to Deal With Both Anthropogenic Forcing and Natural Variability. World Scientific Publ. Co., 2013.
- H. Gildor and E. Tziperman. Sea ice as the glacial cycles' climate switch: Role of seasonal and orbital forcing. *Paleoceanography*, 15(6):605–615, 2000.
- H. Gildor and E. Tziperman. A sea ice climate switch mechanism for the 100-kyr glacial cycles. *J. Geophys. Res.*, 106(C5):9117–9133, 2001.

- H. Gildor, E. Tziperman, and J. R. Toggweiler. Sea ice switch mechanism and glacial-interglacial CO<sub>2</sub> variations. *Glob. Biogeochem. Cyc.*, 16(3):1032, 2002. doi: 10.1029/2001GB001446.
- J. M. Gregory, W. J. Ingram, M. A. Palmer, G. S. Jones, P. A. Stott, R. B. Thorpe, J. A. Lowe, T. C. Johns, and K. D. Williams. A new method for diagnosing radiative forcing and climate sensitivity. *Geophys. Res. Lett.*, 31(3):L03205, 2004. doi: 10.1029/2003GL018747.
- Alan M. Haywood, Aisling M. Dolan, Steven J. Pickering, Harry J. Dowsett, Erin L. McClymont, Caroline L. Prescott, Ulrich Salzmann, Daniel J. Hill, Stephen J. Hunter, Daniel J. Lunt, James O. Pope, and Paul J. Valdes. On the identification of a Pliocene time slice for data–model comparison. *Philosophical Transactions of the Royal Society A: Mathematical, Physical and Engineering Sciences*, 371(2001), 2013.
- IPCC. *Climate Change 2013: The Physical Science Basis. Contribution of Working Group I to the Fifth Assessment Report of the Intergovernmental Panel on Climate Change*. Cambridge University Press, Cambridge, United Kingdom and New York, NY, USA, 2013.
- R. Knutti and G. C. Hegerl. The equilibrium sensitivity of the Earth’s temperature to radiation changes. *Nature Geoscience*, 1(11):735–743, 2008. doi: 10.1038/ngeo337.
- P. Köhler, B. de Boer, A. S. von der Heydt, L. B. Stap, and R. S. W. van de Wal. On the state-dependency of the equilibrium climate sensitivity during the last 5 million years. *Climate of the Past*, 11:1801–1823, 2015. doi: 10.5194/cp-11-1801-2015.
- P. Köhler, R. Bintanja, H. Fischer, F. Joos, R. Knutti, G. Lohmann, and V. Masson-Delmotte. What caused Earth’s temperature variations during the last 800,000 years? Data-based evidence on radiative forcing and constraints on climate sensitivity. *Quat. Sci. Rev.*, 29(1-2):129–145, 2010. doi: 10.1016/j.quascirev.2009.09.026.
- D. J. Lunt, A. M. Haywood, G. A. Schmidt, U. Salzmann, P. J. Valdes, and H. J. Dowsett. Earth system sensitivity inferred from Pliocene modelling and data. *Nature Geoscience*, 3(1):60–64, 2010. doi: 10.1038/ngeo706.
- M. A. Martinez-Boti, G. L. Foster, T. B. Chalk, E. J. Rohling, P. F. Sexton, D. J. Lunt, R. D. Pancost, M. P. S. Badger, and D. N. Schmidt. Plio-Pleistocene climate sensitivity evaluated using high-resolution CO<sub>2</sub> records. *Nature*, 518(7537):49–54, 2015. doi: 10.1038/nature14145.
- E. J. Rohling, A. Sluijs, H. A. Dijkstra, P. Köhler, R. S. W. van de Wal, A. S. von der Heydt, and PALAEOSENS Project members. Making sense of palaeoclimate sensitivity. *Nature*, 491(7426):683–691, 2012. doi: 10.1038/nature11574.
- M. Scheffer, V. Brovkin, and P. M. Cox. Positive feedback between global warming and atmospheric co<sub>2</sub> concentration inferred from past climate change. *Geophysical Research Letters*, 33(10):L10702, 2006. doi: 10.1029/2005GL025044.

- M. Schulz. The tempo of climate change during Dansgaard-Oeschger interstadials and its potential to affect the manifestation of the 1470-year climate cycle. *Geophys. Res. Lett.*, 29(1):1002, 2002. doi: 10.1029/2001GL013277.
- S. E. Schwartz. Determination of earth’s transient and equilibrium climate sensitivities from observations over the twentieth century: Strong dependence on assumed forcing. *Surv. Geophys.*, 33(3):745–777, 2012. doi: 10.1007/s10712-012-9180-4.
- C. A. Senior and J. F. B. Mitchell. The time dependence of climate sensitivity. *Geophys. Res. Lett.*, 27(17):2685–2688, 2000. doi: 10.1029/2000GL011373.
- UNESCO. 10th report of the joint panel on oceanographic tables and standards. Technical Report 36, UNESCO Tech. Pap. in Mar. Sci., 1981.
- A. S. von der Heydt, P. Köhler, R. S. W. van de Wal, and H. A. Dijkstra. On the state dependency of fast feedback processes in (paleo) climate sensitivity. *Geophysical Research Letters*, 41(18):6484–6492, 2014. doi: 10.1002/2014GL061121.
- M. Yoshimori, J. C. Hargreaves, J. D. Annan, T. Yokohata, and A. Abe-Ouchi. Dependency of feedbacks on forcing and climate state in physics parameter ensembles. *Journal of Climate*, 24:6440–6455, 2011. doi: 10.1175/2011JCLI3954.1.



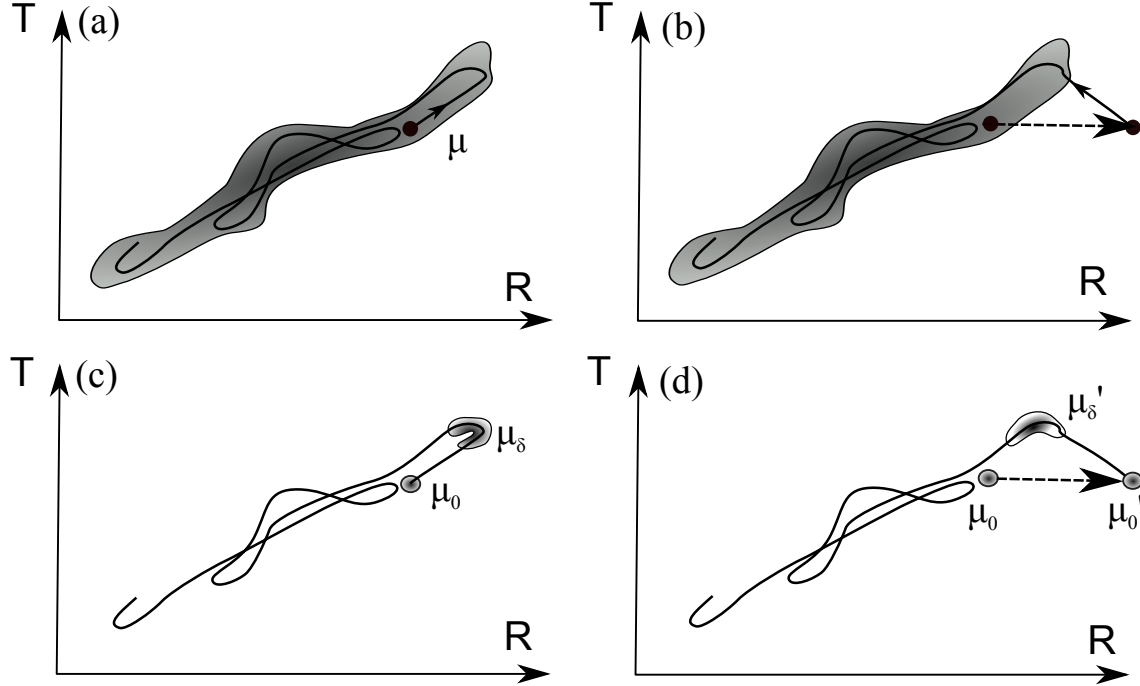


Figure 1: Schematic diagram showing global mean temperature  $T$  versus radiative forcing  $R$  due to atmospheric  $\text{CO}_2$ . (a) In the presence of natural forcing we assume there is a stationary distribution  $\mu$  in the  $(T, R)$  plane - this is the projection of a dynamical measure onto this plane. Picking two points relative to this measure gives a distribution of slopes that represent long-term variability of climate sensitivity for this forcing. (b) An impulsive change in  $\text{CO}_2$  at some point results in a change of  $R$  (dashed line) that takes the system state away from the attractor. If the perturbation is not too large then, after a transient (small arrow), we expect to continue to explore the plane according to the distribution  $\mu$ . (c) Starting at a particular distribution  $\mu_0$  we examine how  $\mu_0$  evolves under the dynamics over time  $\delta > 0$  to a new distribution  $\mu_\delta$ . Over very long timescales will can be expected to approach the stationary distribution  $\mu$  in the  $(T, R)$  plane. Picking start and end points relative  $\mu_0$  and  $\mu_\delta$  respectively gives a distribution of slopes that represent the variability of climate sensitivity for this forcing over this time interval. (d) An impulsive change in  $\text{CO}_2$  at some point results in a change of  $R$  (dashed line) moves the initial distribution  $\mu_0$  to a new location  $\mu'_0$  away from the attractor. After time  $\delta > 0$  we reach a perturbed distribution  $\mu'_\delta$  that, if  $\delta$  is large enough, can be approximated by  $\mu_\delta$ .

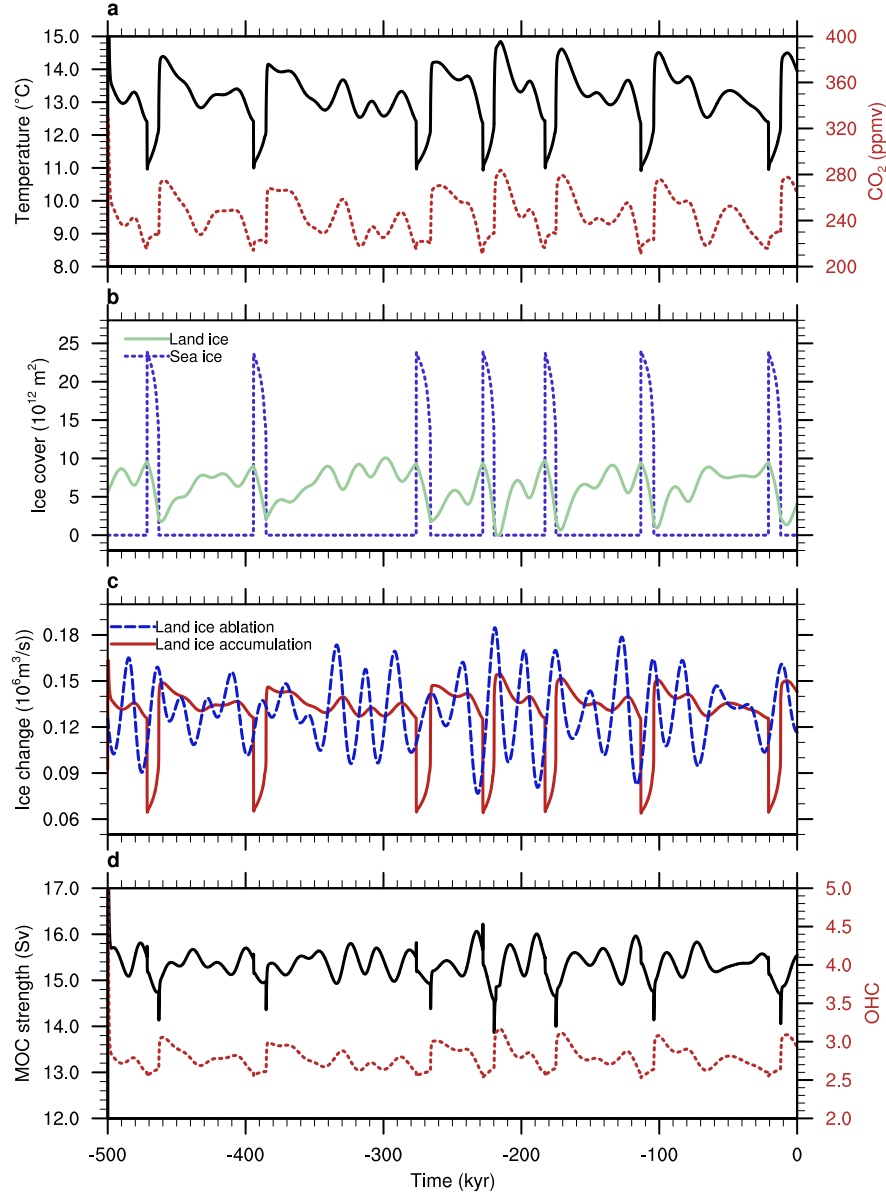


Figure 2: Glacial cycles of the box model, shown are time series of 100-year averages. (a) Simulated global mean surface temperature  $T$  (black line) and atmospheric  $\text{CO}_2$  (red line); (b) Land ice (green line) and sea ice (blue line) cover of the northern polar box; (c) Land ice accumulation (red line) and ablation (blue line) in the northern polar box; (d) Strength of the ocean meridional overturning circulation (black line), measured as the volume exchange between surface and deep northern polar ocean boxes and ocean heat content (red line).

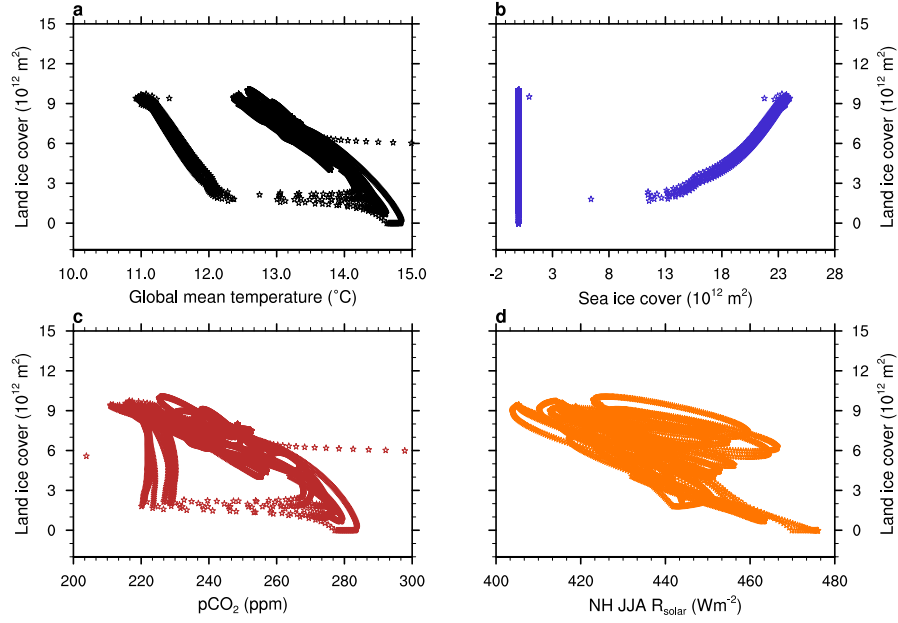


Figure 3: Phase diagrams of the glacial cycles of the box model; each point is a 100-year average. (a) NH land ice cover as a function of global mean temperature; (b) NH land ice cover as a function of NH sea ice cover; (c) NH land ice cover as a function of atmospheric  $\text{CO}_2$  concentration  $p\text{CO}_2$ ; (d) NH land ice cover as a function of orbital variations in solar radiation  $R_{\text{solar}}$  defined as summer insolation (JJA) over the northern polar box of the model ( $45\text{-}90^{\circ}$  averaged).

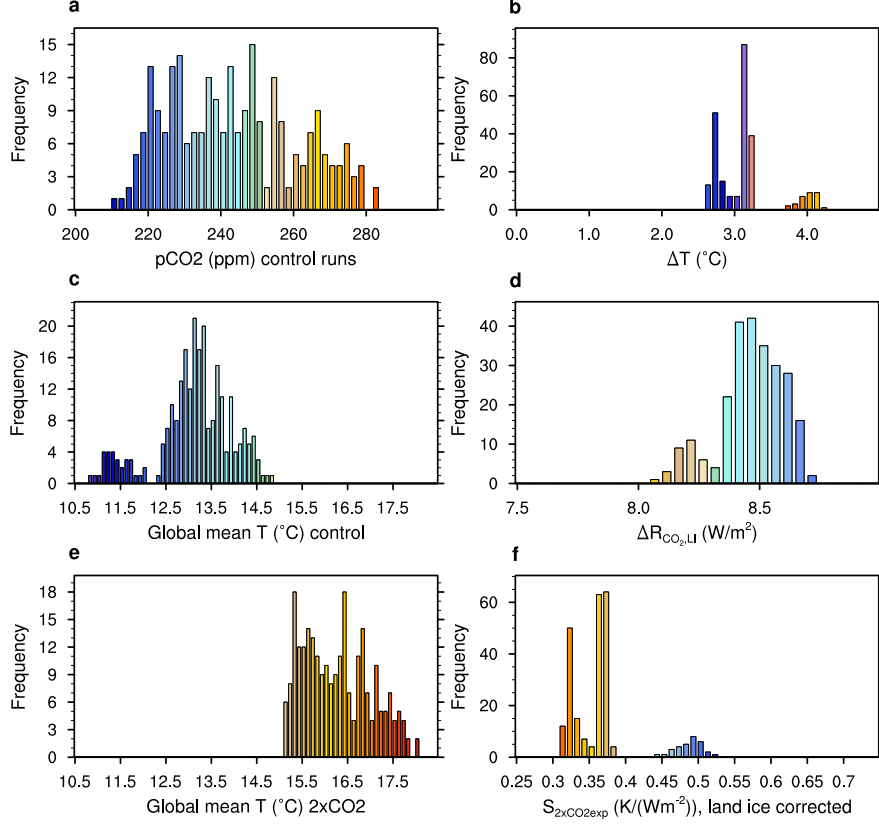


Figure 4: Classical model-determined climate sensitivity. CO<sub>2</sub> is prescribed and doubled within 30 years and held fixed afterwards until year 200. Ensemble starting from 250 initial conditions taken from the glacial-interglacial time series (500 kyr, shown in Fig. 2a). Climate sensitivity is determined following eq. 9 and corrected for land ice changes (eq. 5). (a) Distribution of initial atmospheric CO<sub>2</sub>-concentrations in the ensemble; (b) Distribution of temperature change between doubled CO<sub>2</sub> and control simulation (difference is taken between the averages of the last 10 years of each simulation); (c) Distribution of the initial global mean temperature; (d) Distribution of the radiative forcing  $R_{[CO_2,LI]}$  change between doubled CO<sub>2</sub> and control simulation (difference is taken between the averages of the last 10 years of each simulation); (e) Distribution of the global mean temperature (average of the last 10 years of simulation) after doubling of CO<sub>2</sub>; (f) Distribution of  $S_{2 \times CO_2 exp}$ .

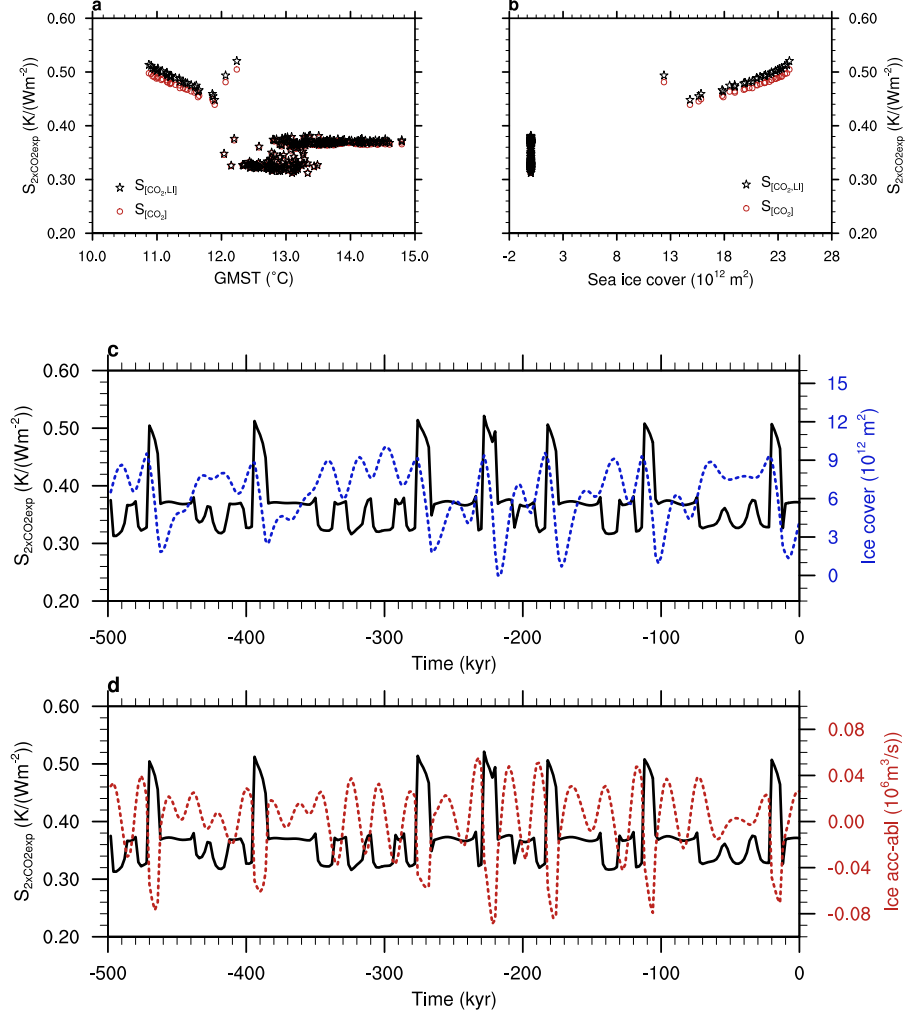


Figure 5: State dependence of the model-determined climate sensitivity under prescribed CO<sub>2</sub> (see Fig. 4). (a)  $S_{2 \times CO_2 exp}$  versus global mean temperature. Note the higher sensitivity during colder climates; (b)  $S_{2 \times CO_2 exp}$  versus NH sea ice cover; (c) Time series of  $S_{2 \times CO_2 exp}$  (black line, left axis) and NH land ice cover (blue dotted line, right axis); (d) Time series of  $S_{2 \times CO_2 exp}$  (black line, left axis) and NH land ice change (accumulation minus ablation, red dotted line, right axis).

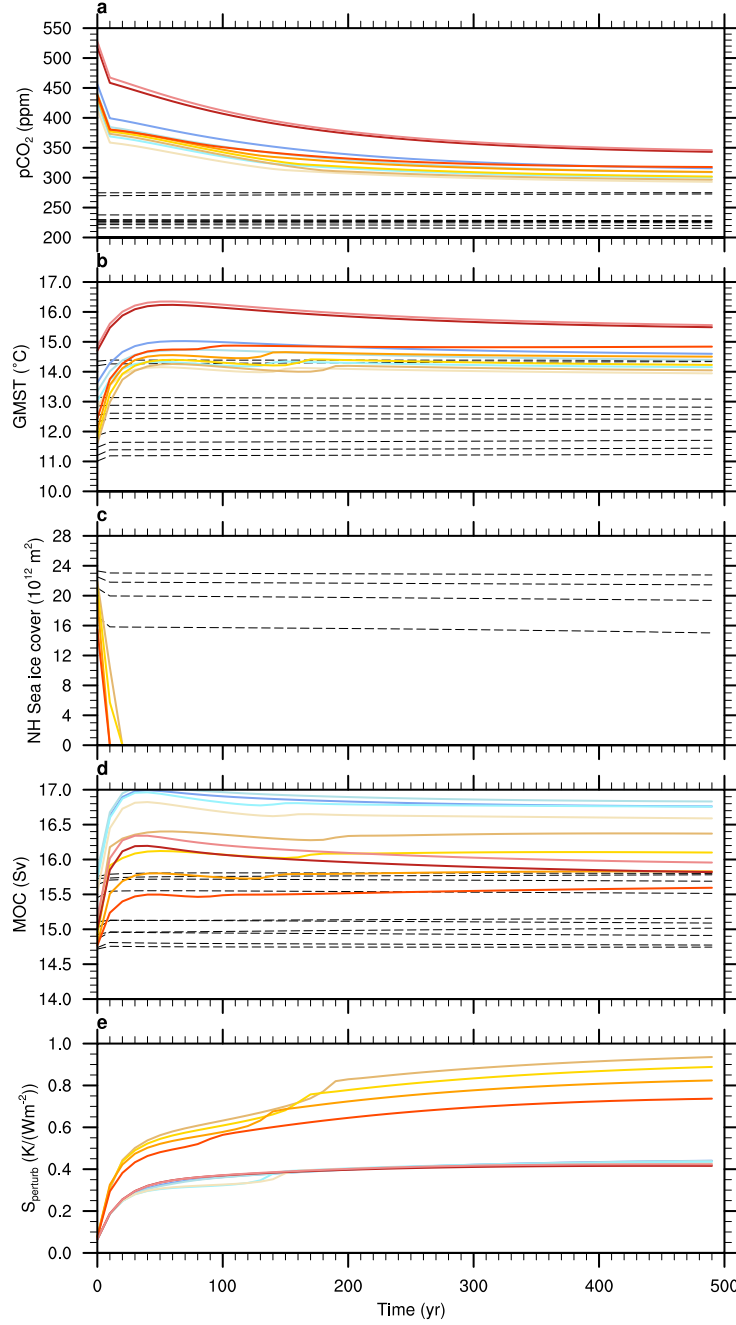


Figure 6: Climate sensitivity  $S_{perturb}$  from perturbation experiments with dynamical CO<sub>2</sub>. Shown are time series of experiments, where CO<sub>2</sub> is doubled initially and free to evolve until year 500 (coloured lines) along with the control experiments, where CO<sub>2</sub> is not doubled initially (black dashed lines). The ensemble starts from 250 initial conditions taken from the glacial-interglacial time series (500 kyr, shown in Fig. 2a). In this figure we show 10 ensemble members. Climate sensitivity is determined following eq. 10. (a) Atmospheric CO<sub>2</sub>; (b) Global mean surface temperature; (c) Northern hemisphere sea ice fraction; (d) Strength of the ocean meridional overturning circulation; (e)  $S_{perturb}$ .

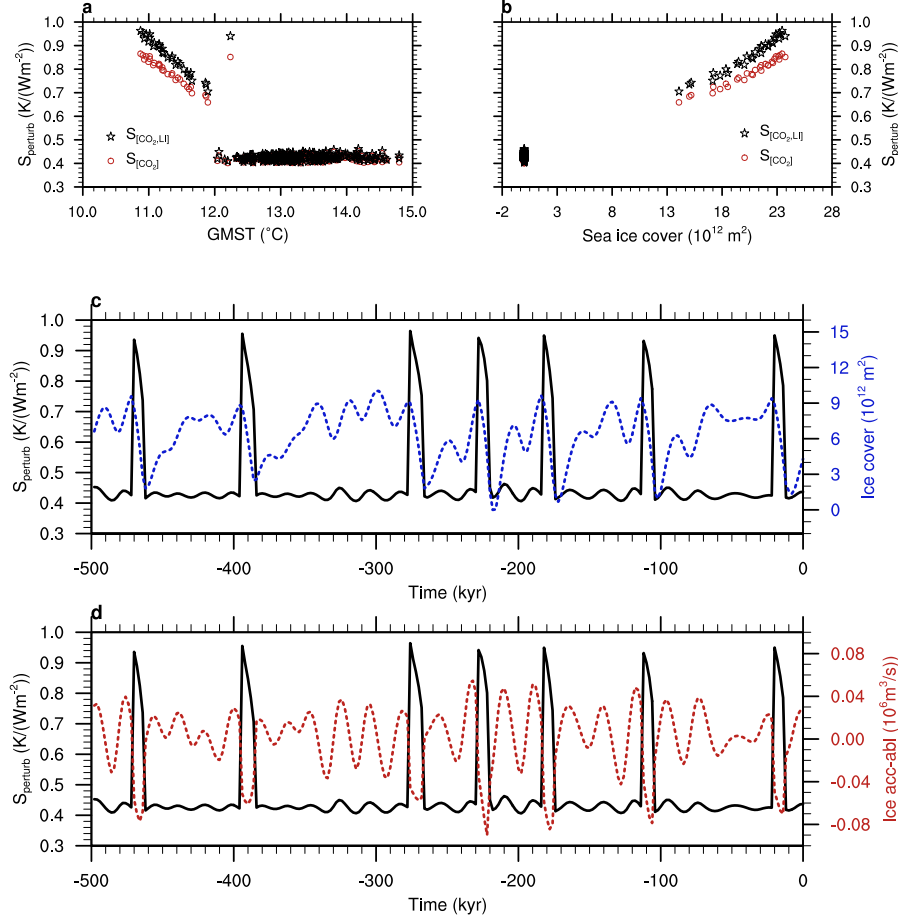


Figure 7: State dependence of the climate sensitivity  $S_{perturb}$  from the perturbation experiments (Fig. 5). Climate sensitivity is determined following eq. 10. (a)  $S_{perturb}$  versus global mean temperature; (b)  $S_{perturb}$  versus NH sea ice cover; (c) Time series of  $S_{perturb}$  (black line, left axis) and NH land ice cover (blue dotted line, right axis); (d) Time series of  $S_{perturb}$  (black line, left axis) and NH land ice change (accumulation minus ablation, red dotted line, right axis).

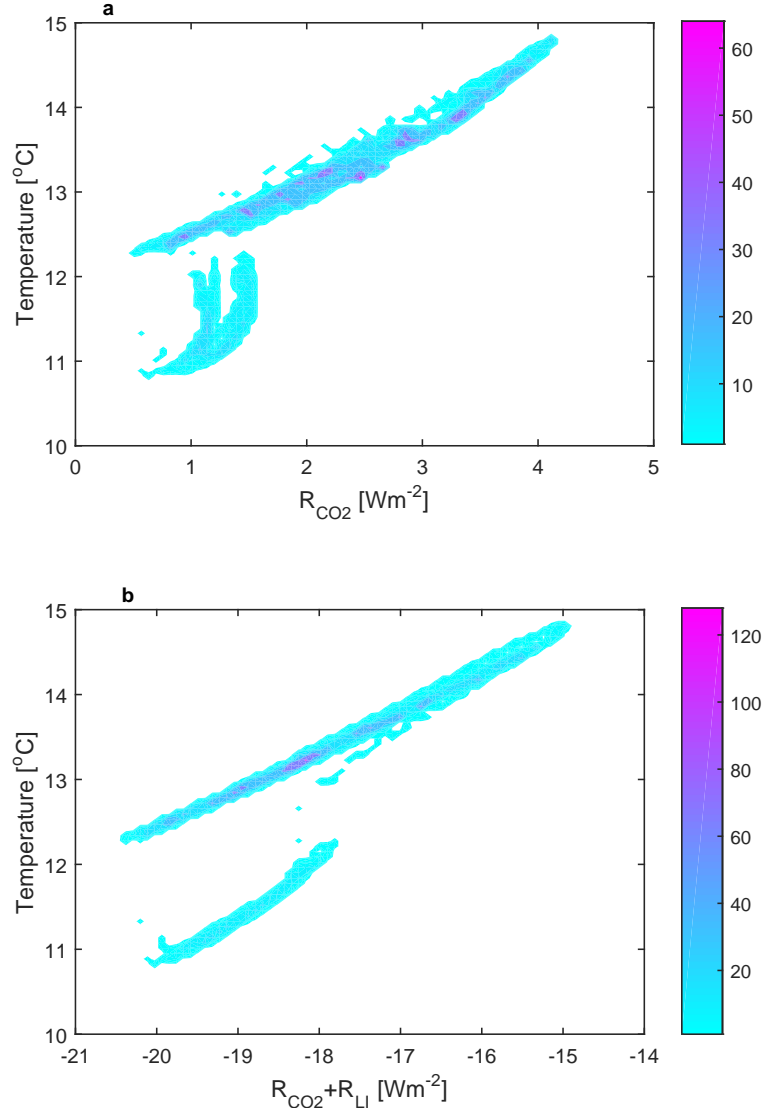


Figure 8: Relation between global mean temperature and radiative contributions due to pCO<sub>2</sub>  $R_{[CO_2]}$  and land ice  $R_{[LI]}$  (slow feedback). Colours [a.u.] show an approximation of the probability density of distribution of these relations, where a transient has been removed. (a) Global mean surface temperature versus  $R_{CO_2}$ ; (b) Global mean surface temperature versus  $R_{CO_2,LI}$ .



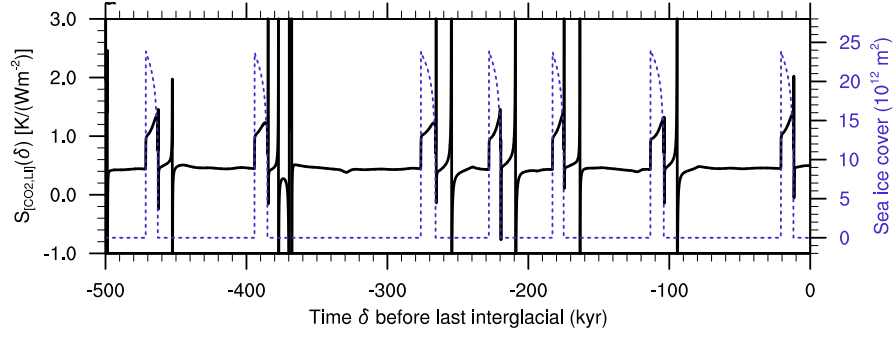


Figure 9: Equilibrium climate sensitivity approximated by the specific climate sensitivity  $S_{[CO_2,LI]}(\delta)$  as derived from the long glacial-interglacial simulation by comparing each point in time to the models *preindustrial* climate at  $t_{ref} = 0$ , according to Eq. (11), where  $\delta$  is the time before  $t_{ref} = 0$ . The blue dashed line represents the sea ice cover.

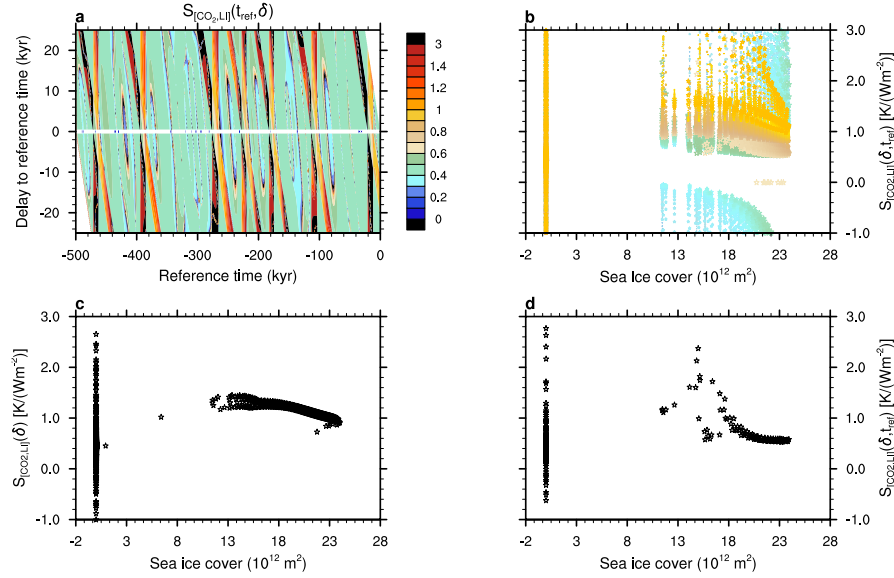


Figure 10: Equilibrium climate sensitivity approximated by the specific climate sensitivity  $S_{[CO_2,LI]}(\delta, t_{ref})$  as derived from the long glacial-interglacial simulation according to Eq. (11). All reference times along the time series are considered and delays to the reference time between  $\delta = -25 \dots +25$  kyr (about half a glacial-interglacial period). (a) Contour plot of  $S_{[CO_2,LI]}(\delta, t_{ref})$  as a function of  $\delta$  and  $t_{ref}$ . Black shading indicates values of  $S_{[CO_2,LI]}(\delta, t_{ref})$  above  $3 \text{ K (W m}^{-2})^{-1}$  or below 0; (b)  $S_{[CO_2,LI]}(\delta, t_{ref})$  as a function of sea ice cover. The largest symbols reflect the smallest delays  $\delta$  and green-blue (brown-yellow) colors indicate negative (positive) delays; (c)  $S_{[CO_2,LI]}(\delta)$  for a fixed  $t_{ref} = 0$  as a function of NH sea ice cover; (d)  $S_{[CO_2,LI]}(t_{ref})$  for a fixed delay  $\delta = 500$  yr as a function of NH sea ice cover.

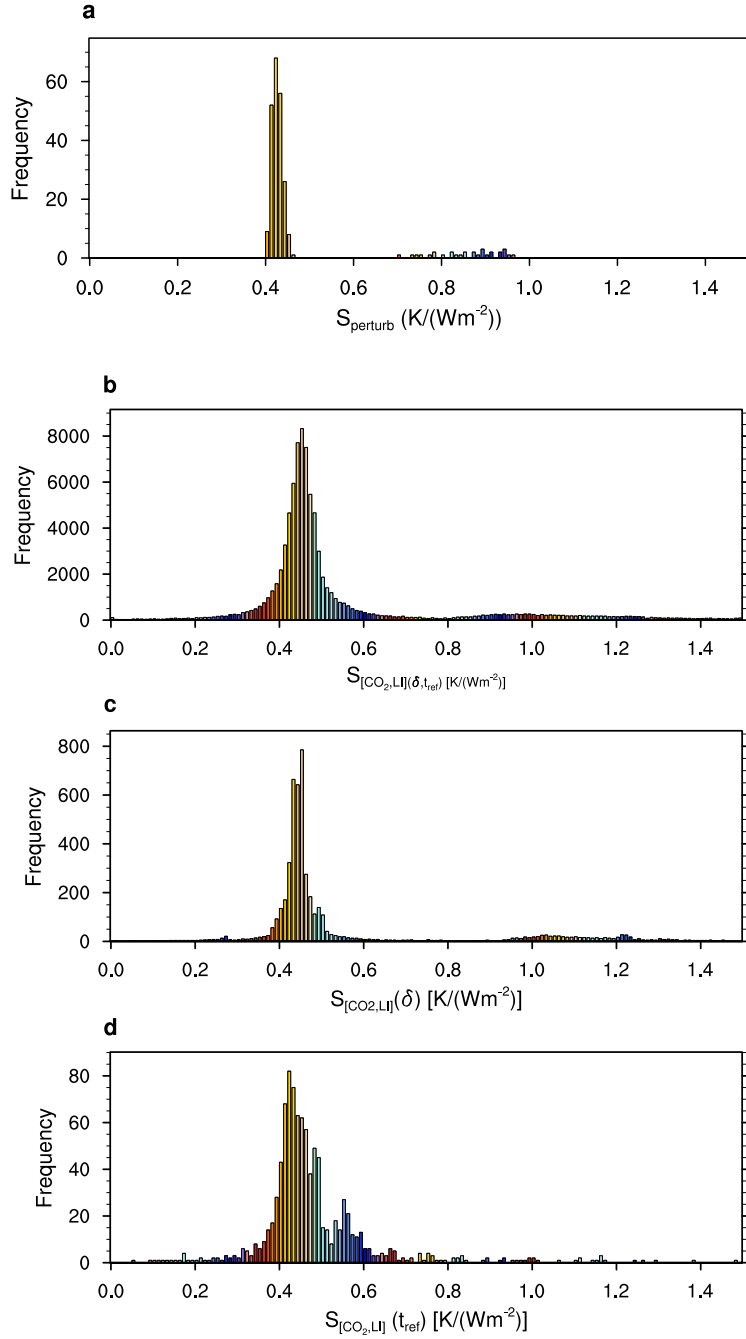


Figure 11: Distributions of climate sensitivity as derived following the different approaches in this paper. All sensitivities reflect the specific climate sensitivity  $S_{[\text{CO}_2, \text{LI}]}$ . (a) Distribution of  $S_{\text{perturb}}$  (after 500 years), see Fig. 7; (b) Distribution of  $S_{[\text{CO}_2, \text{LI}]}(\delta, t_{\text{ref}})$  for delays  $\delta = -25 \dots +25$  kyr as shown in Fig. 10a; (c) Distribution of  $S_{[\text{CO}_2, \text{LI}]}(\delta)$  for a fixed reference time ( $t_{\text{ref}} = 0$ ); (d) Distribution of  $S_{[\text{CO}_2, \text{LI}]}(t_{\text{ref}})$  for a fixed delay ( $\delta = 500$  yr).